University of Szeged
Faculty of Medicine, Faculty of Science and Informatics
Department of Medical Physics and Informatics

PhD Thesis

The evolution of spreading depolarization in response to osmotic or ischemic challenge in rat brain slices

Rita Frank

Supervisors: Dr. Ákos Menyhárt
Dr. Eszter Farkas

Doctoral School of Theoretical Medicine

Szeged, 2021

Publications related to the PhD thesis

Rita Frank, Ferenc Bari, Ákos Menyhárt, Eszter Farkas

Comparative analysis of spreading depolarizations in brain slices exposed to osmotic or metabolic stress.

BMC Neuroscience 2021 May 3;22(1):33. doi: 10.1186/s12868-021-00637-0.

Scimago classification: Neuroscience/Neuroscience (miscellaneous) - Q2

Ákos Menyhárt [a], Rita Frank [a], Attila E. Farkas, Zoltán Süle, Viktória É. Varga, Ádám Nyúl-Tóth, Anne Meiller, Orsolya Iványkovits-Kiss, Coline L. Lemale, Írisz Szabó, Réka Tóth, Dániel Zölei-Szénási, Johannes Woitzik, Stephane Marinesco, István A. Krizbai, Ferenc Bari, Jens P. Dreier, Eszter Farkas

[a]These authors contributed equally to this work.

Malignant astrocyte swelling and impaired glutamate clearance drive the expansion of injurious spreading depolarization foci

Journal of Cerebral Blood Flow and Metabolism August 24, 2021., DOI: 10.1177/0271678X211040056

Scimago classification: Neuroscience/Neurology - D1

Contents

Publications related to the PhD thesis 1

Abbreviations 5

1. Introduction 6

1.1. Ischemic stroke and primary injury 6

1.2. Detrimental effects and underlying mechanisms of spreading depolarization 6

1.3. Edema formation during ischemic stroke 8

1.4. Astrocytic regulation of neuronal excitability 10

1.5. Acute brain slice as a model system in neuroscience research 11

1.6. Aims of the study 12

2. Materials and methods 13

2.1. Animals 13

2.2. Brain slice preparations 13

2.3. Local field potential recordings 13

2.4. Intrinsic optical signal imaging 14

2.5. Comparative analysis of spreading depolarizations under osmotic or metabolic stress 14

2.5.1. Methods of SD elicitation 14

2.5.2. Histology 16

2.6. Observation of simultaneous depolarization on brain slices 17

2.6.1. Experimental protocols 17

2.6.2. Pharmacological treatments 17

2.6.3. Measurement of extra-synaptic glutamate concentration 18

2.6.4. Histology 19

Golgi-Cox staining 19

Electron microscopy 19

2.7. Data analysis 19

3. Results 22

3.1. Comparative analysis of spreading depolarizations under osmotic or metabolic stress 22

3.1.1. Prolonged SDs occur upon acute osmotic stress and in response to oxygen-glucose deprivation 22

3.1.2. Severe osmotic stress and oxygen glucose deprivation enhance the area invaded by SD 23

3.1.3. Oxygen-glucose deprivation and osmotic stress restrain cell survival after SD 25

3.2. Observation of simultaneous depolarization on brain slices 26

3.2.1. Hypo-osmotic stress favors the evolution of SiD 26

3.2.2. Astrocyte swelling is implicated in SiD 29

3.2.3. SiD evolution promotes lesion maturation 32

3.2.4. Inhibition of astrocyte swelling or volume regulated glutamate release alleviates tissue edema and prevents SiD 32

3.2.5. Hyperosmotic treatment reverses tissue swelling, restores physiological extracellular glutamate concentration, and prevents SiD 36

4. Discussion 38

4.1. Comparative analysis of spreading depolarizations under osmotic or metabolic stress 38

4.1.1. Relevance of the applied experimental approaches 39

4.1.2. SDs under osmotic and metabolic stress invaded extended cortical area and reduced cellular viability 40

4.1.3. SDs elicited by various stimuli represent different stages of the SD continuum 41

4.2. Observation of simultaneous depolarization in brain slices 42

4.2.1. SiD is the pathological expansion of prior SD foci in brain slices exposed to osmotic stress 43

4.2.2. Astrocyte swelling plays a key role in the evolution of SiD 43

5. Main observations and conclusions..... 45

6. Summary 46

7. References 48

Abbreviations

aCSF: artificial cerebrospinal fluid

AMPA: α-amino-3-hydroxy-5-methyl-4-isoxazolepropionic acid

ANOVA: analysis of variance

AQP4: aquaporin-4 channel

AUC: area under the curve

BBB: blood brain barrier

BSA: bovine serum albumin

Bum: Bumetanide

CBF: cerebral blood flow

CCD: charge-coupled device

CNS: central nervous system

DC: direct current

EAAT2: excitatory amino acid transporter2

EEG: electroencephalography

ES: electric stimulation

EVP: evoked field potential

FC: fluorocitrate

GABA: α-aminobutyric acid

HM: hypo-osmotic medium

HRM: hyper-osmotic solution

ICP: intracranial pressure

IOS: intrinsic optical signal

LFP: local field potential

MCAO: middle cerebral artery occlusion

NKCC: $Na^+/K^+/Cl^-$ co-transporter

NMDA: N-methyl D-aspartate

OGD: oxygen-glucose deprivation

PBS: phosphate buffered saline

PFA: paraformaldehyde

PPD: poly-m-phenylenediamine

rCBF: regional cerebral blood flow

ROI: region of interest

rSD: recurrent spreading depolarization

SD: spreading depolarization

SiD: simultaneous depolarization

stdev: standard deviation

TBI: traumatic brain injury

TTC: 2,3,5-triphenyltetrazolium chloride

V_o: extracellular potential

VRAC: volume-regulated anion channel

WHO: World Health Organization

1. Introduction

1.1. Ischemic stroke and primary injury

Approximately 15 million people suffer a stroke every year, the World Health Organization (WHO) classifies stroke as the second leading cause of death and the third leading cause of long-term disability worldwide[1]. Stroke is the rapid evolution of a focal neurologic deficit induced by a disruption of blood supply to the corresponding brain region. Stroke cases can either be ischemic (an occlusion of an artery) or hemorrhagic (a leakage of an artery)[1]. Ischemic stroke is accountable for 87 % of all stroke cases and has been classified into subtypes according to the mechanism of injury. These subtypes are: large-artery atherosclerosis, cardiogenic emboli and small vessel occlusive disease. The ischemic area can be separated into two major parts according to the viability and salvageability of the nervous tissue. In the ischemic core region, the perfusion is severely decreased (blood flow: 10-25 % relative to normal baseline), neurons and glial cells undergo rapid necrosis[2]. The core is surrounded by the penumbra region where residual blood flow persists, and the local cerebral blood flow (CBF) ranges between 20-40 % relative to baseline. The penumbra contains electrophysiologically inactive but viable and, most importantly, salvageable cells, which places it in the center of ischemic neuroprotective therapy[2].

1.2. Detrimental effects and underlying mechanisms of spreading depolarization

Spreading depolarization (SD) is a slowly propagating wave of near complete neuronal and glial depolarization followed by temporary suppression of brain electrical activity[3, 4]. After ischemia onset, SD first develops in the core region[3, 4], this initial SD affects not just the core, but spreads through the ipsilateral cortex in a radial pattern. SD was first described by the Brazilian neurobiologist Aristides Leão in 1944[5]. He observed the spreading depression of spontaneous electroencephalographic (EEG) activity after the repetitive stimulation of the rabbit cerebral cortex to trigger seizures. The spreading depression of spontaneous cortical activity lasted for several minutes[6] and it was associated with a large negative shift of the slow cortical or direct current (DC) potential[7]. SD has been recognized to propagate from a punctual focus and spreads through the cerebral grey matter at a rate of 2-6 mm/minute. The minimum tissue volume of the SD focus was estimated to be ~1 mm^3 *in vivo*, or even smaller, ~0.03–0.06 mm^3 *in vitro*[8-10]. The duration of SDs is mainly determined by the residual perfusion[6] . In the penumbra, SDs display prolonged duration while in non-ischemic regions SDs appear as

depolarizations with short duration and complete recovery. As time passes by, recurrent SDs arise due to metabolic supply–demand mismatch in the penumbra[7, 11] or even in more distant cortical areas with impaired metabolism but preserved excitability (Fig. 1)[12].

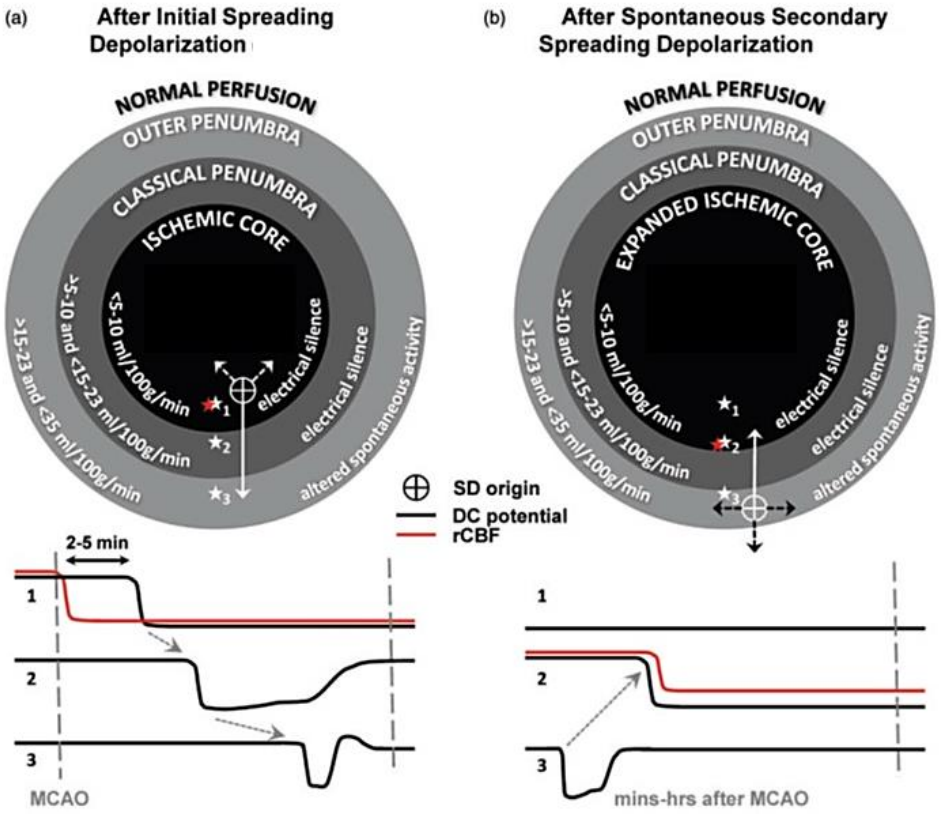

Figure 1. Lesion progression during experimental focal ischemia. Schematic drawings illustrate various zones of ischemia in the cerebral cortex after middle cerebral artery occlusion (MCAO). Characteristic changes in DC potential recordings (black) and in regional cerebral blood flow (rCBF; red) are taken at the three monitoring locations indicated by stars. (**a)** Diagram depicts the status of ischemic zones right after the passage of the initial spreading depolarization. The first depolarization spreads through the penumbra (white arrows) into distant, normally perfused tissue areas. **(b)** Minutes, hours, or even days after stroke onset SDs arise repeatedly in the penumbral hot zones as a result of metabolic crisis. These recurrent depolarizations (rSD) propagate both outward from and inward to the ischemic core and contribute to infarct development in a stepwise manner after the passage of each SD. (Source: Jed A. Hartings *et al*., 2017[13]).

Massive transmembrane ion movements are typical of SD, such as a rapid increase in $[K^+]_e$ to 30–60 mM, a decrease in $[Na^+]_e$ and $[Cl^-]_e$ to 50–70 mM and in $[Ca^{2+}]_e$ to 0.2–0.8 mM (Fig. 2)

can be observed[14]. Moreover, several amino acids, such as glutamate and aspartate are released during SD[14].

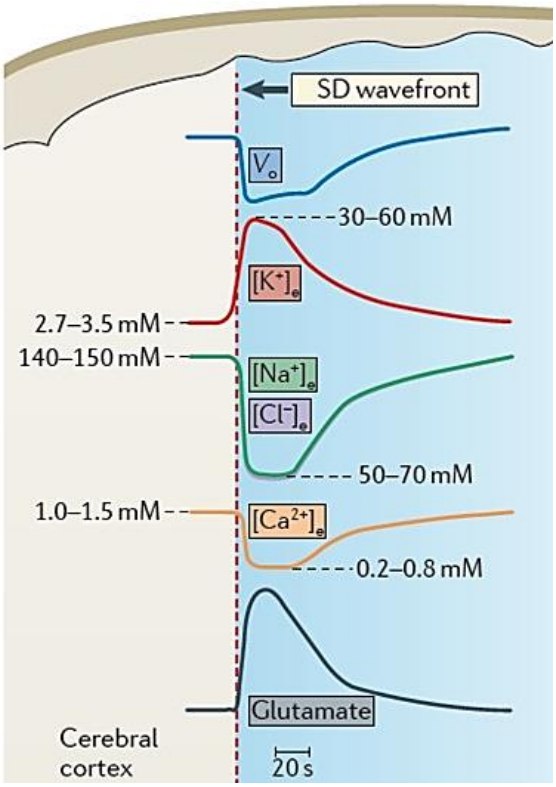

Figure 2. SD-related transmembrane ionic changes. Changes in the extracellular concentrations of K^+ ($[K^+]_e$), Na^+ ($[Na^+]_e$), Cl^- ($[Cl^-]_e$), Ca^{2+} ($[Ca^{2+}]_e$) and of glutamate during SD. Rapid extracellular potential (V_o) change during the initial phase of SD is accompanied by a rapid $[K^+]_e$ increase and decrease of $[Na^+]_e$ and $[Cl^-]_e$ and $[Ca^{2+}]_e$. The depolarization and the associated ionic changes propagate across the cerebral cortex. Red dashed line represents the SD wavefront. (Source: Daniela Pietrobon and Michael A. Moskowitz, 2014[14]).

In metabolically compromised tissue the frequency and duration of SDs are in strong correlation with secondary injury development[7, 15, 16]. In experimental models of focal cerebral ischemia, repeated SDs cause enhanced infarct volume, thus SD can be considered as an electrophysiological biomarker of injury progression[17]. Accordingly, pharmacological reduction of SD frequency and/or duration could achieve neuroprotection[13, 18, 19]. However, SDs in healthy, adequately supplied tissue may not cause direct damage, although SD has been implicated in the activation of trigeminal circuits and the evolution of migraine headache[20-22].

1.3. Edema formation during ischemic stroke

Brain edema frequently manifests after the onset of cerebrovascular disorders such as ischemic stroke[23] and traumatic brain injury (TBI) and worsens the clinical outcome by increasing intracranial pressure (ICP)[24]. Cerebral edema after ischemic stroke has been divided into three major states: cytotoxic, ionic and vasogenic edema[25] (Fig. 3). Cytotoxic edema is defined by intracellular water accumulation without blood brain barrier (BBB) opening, which occurs within minutes after the cessation of CBF. This initial swelling is triggered by ATP depletion and is characterized as swelling of astrocytes and neuronal dendrites[26]. During SD, the absence of oxygen and glucose supply induces a disruption of transmembrane ion gradients and leads

to the entry of ions and water into the cells[27]. Later, the intensified metabolic crisis transforms cytotoxic edema to ionic edema that lead to altered endothelial ionic gradients, including the transcapillary flux of Na^+ to the brain parenchyma[28, 29]. Moreover, shear stress after reperfusion results in early, transient leakage of BBB and additional water entry[30]. At this point astrocytes remain swollen and neuronal death starts. Finally, ionic edema transforms to vasogenic edema, in which the complete disruption of cerebrovascular endothelial tight junctions leads to increased BBB permeability to albumin and other plasma proteins at the injured brain region[25]. Since, aquaporin-4 (AQP4), the most common water channel in the brain is mainly located on astrocytic endfeet, astrocytes have a critical role in the maintenance of brain water homeostasis[27, 31, 32]. In experimental models of focal cerebral ischemia, the swelling of astrocytes was persistent and correlated with the total duration of spreading depolarization in the ischemic penumbra[33]. Furthermore, astrocyte soma swelling increased in a stepwise fashion following spontaneous SD, in contrast with the healthy tissue in which SD induced reversible glial swelling[33].

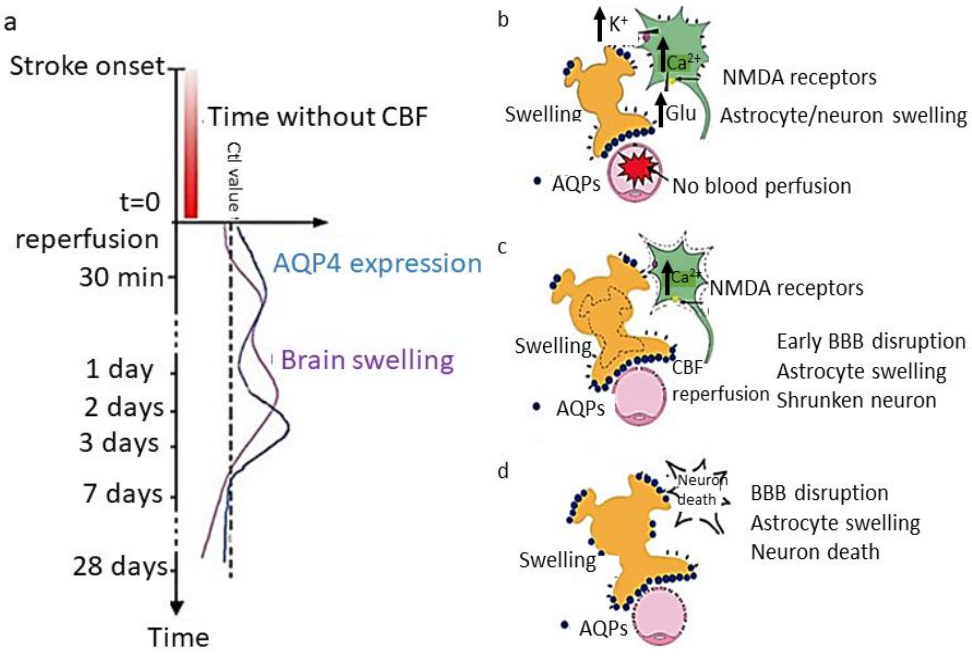

Figure 3. Schematic illustration of edema formation after ischemic stroke (a) Timeline shows edema development after ischemic stroke, blue curve indicates AQP4 expression, purple curve depicts brain swelling after ischemia. **(b)** Cytotoxic edema is characterized as swelling of astrocytes and neuronal dendrites due to the disruption of ion gradients and the entry of ions followed by water influx resulting in cellular swelling mainly through AQP4 channels. **(c)** Ionic edema refers to swollen astrocytes, neuronal death and the leakage of the BBB. **(d)** Vasogenic edema is associated with the disruption of tight junctions between endothelial cells, increased permeability of albumin and other plasma proteins further swelling of astrocytes and subsequent neuronal cell death (Source: J. Badaut et al. 2011[32]).

1.4. Astrocytic regulation of neuronal excitability

Astrocytes are essential for neurons and the brain to function optimally, these cells serve supply of nutrients to neurons, control extracellular ionic gradients and play a role in the modulation of BBB permeability. Moreover, astroglia couple local blood supply to neuronal activity and lower the amount of reactive oxygen species[34]. Importantly, as participants of the tripartite synapse, astrocytes modulate synaptic transmission and neuronal excitability. Astrocytes uptake ions such as potassium, synaptically-released neurotransmitters like glutamate, α-aminobutyric acid (GABA) and glycine, metabolize them and release their precursors back to neurons.

The mechanisms of glial K^+ transport are categorized as K^+ uptake and spatial buffering[35, 36]. During K^+ uptake, excess K^+ ions are temporarily taken up by glial cells by transporters or through K^+ channels[37]. In order to maintain electroneutrality astrocyte K^+ uptake is accompanied by either influx of anions such as Cl^- or by efflux of cations like Na^+. Via spatial buffering of K^+[38], functionally and anatomically coupled glial cells transfer K^+ ions from regions with elevated extracellular K^+ to regions of low extracellular K^+ concentrations[37]. The K^+ current is driven by the difference between the membrane potential of glial syncytium and the local equilibrium potential of K^+.

The bumetanide-sensitive $Na^+/K^+/Cl^-$ co-transporter-1 (NKCC1) is particularly implicated in K^+-induced astrocyte swelling. NKCC1 is expressed by astrocytes in all brain regions and its activity is intensified after ischemia[39, 40]. *In vitro* cultured primary astrocytes demonstrated that NKCC1 contributes to cell swelling in conditions of high extracellular K^+[41]. Further, *in vivo* swelling is attenuated with the NKCC1 inhibitor bumetanide after brain trauma and ischemia[29, 42].

The control of glutamate clearance is also essential for the modulation of neuronal excitability by astroglia. Glutamate is the most common excitatory neurotransmitter in the central nervous system (CNS)[43, 44]. The released glutamate during synaptic transmission must be rapidly cleared from the extracellular space. If high glutamate concentration (>20 μM) persists, this leads to neuronal hyper-excitation and subsequent neuronal death in a process called "glutamate excitotoxicity". Only 20 % of glutamate binds to postsynaptic neuronal receptors[45-47], while the majority of synaptically-released glutamate (80 % or more) diffuses out of the synaptic cleft and is cleared from the extracellular space by astrocytic excitatory amino acid transporter-1 (EAAT-1) and EAAT-2[45, 48]. Glutamate uptake is one of the highest energy-consuming mechanisms in the brain, it uses more than 1 ATP molecule for each molecule of glutamate transported[49]. Under pathological conditions (e. g. ischemia) when ATP is depleted and the

extracellular K^+ is elevated, glutamate transporters change to reverse mode and release glutamate[50]. In case of brain edema swollen astrocytes release glutamate as osmolyte to the extracellular space via volume regulated anion channels (VRACs)[51, 52].

As a result of the arrested astrocytic uptake of K^+ and glutamate, neurons fail to maintain the resting ion gradients across their cell membrane and become susceptible for increased action potential firing, epileptiform activity and SD. In our previous *in vivo* experiments we observed that the focus of an SD event became extensive rather than punctual and affected simultaneously an enlarged tissue area during acute ischemic tissue swelling[53].

1.5. Acute brain slice as a model system in neuroscience research

Acute brain slice preparations have been used since 1950s for modelling a variety of neurological disorders, investigating synaptic activity and testing neurochemical agents[54]. *In vitro* brain slices have been suitable to recapitulate the neurophysiological hallmarks of SD accurately[4], and offer the opportunity to explore these changes free of cerebrovascular interferents[55]. The latter feature is especially pertinent when conducting optical imaging. Further, manipulations of the composition of the medium over the preparation allows the controlled simulation of global cerebral ischemia (e.g. oxygen glucose deprivation, OGD)[55], tissue acidosis (e.g. changing the bicarbonate or CO_2 content of the medium)[56], or tissue swelling (e.g. hypo-osmotic medium, HM)[57]. Also, the application of pharmacological agents may yield highly reproducible, consistent data due to the uniform conditions, to aid the mechanistic understanding of SD evolution. For example, specific ion channels, exchangers or transporters mediating ion currents or amino acid translocations with SD may be studied effectively[53, 58-61]. Brain slice preparations are an ideal, basic experimental model to test the efficacy of SD inhibiting agents (e.g. N-methyl D-aspartate (NMDA) or sigma-1 receptor blockers) with the goal to achieve neuroprotection[62, 63]. Finally, brain slices yield the opportunity to study different anatomical regions such as cortex, hippocampus, striatum, subcortical gray matter or brain stem. However, cutting through neural pathways is inevitable during preparation which impedes the examination of complex signaling circuits in brain slices.

1.6. Aims of the study

Based on the above, we hypothesized, that;

I. SDs are more injurious in severely compromised tissue and significantly decrease the viability of brain tissue;

II. Astrocyte dysfunction due to acute tissue swelling leads to potassium and glutamate accumulation and contribute to ischemic lesion progression.

In order to prove the presented hypotheses, the following aims were formulated;

I. We set out to provide a comparative evaluation of SD evolution in live brain slices, in response to selected SD triggers and in various media, under otherwise standardized experimental conditions.

We examined electrophysiological characteristics together with the intrinsic optical signal features of SDs under global oxygen-glucose deprivation or osmotic stress with respect to the physiological condition. We pay particular attention here to spatial SD features, such as the volume of the area engaged in SD and the focal area of SD.

II. We set out to define the role of astrocytes in the evolution of acute tissue swelling as was seen in acute cerebral ischemia *in vivo*, and examine astrocytic glutamate clearance by extracellular glutamate measurements.

To achieve our goals, we used local field potential (LFP) measurements and intrinsic optical signal (IOS) imaging techniques to assess the temporal and spatial characteristics of SD at mesoscopic scale (mm, whole slice). Histological techniques were applied to explore the effect of SD on tissue viability in different experimental conditions. Pharmacological means were applied to investigate the implication of astrocytes in tissue swelling. Finally, enzymatic glutamate biosensors were used to measure extracellular glutamate levels.

2. Materials and methods

2.1. Animals

The experimental procedures were approved by the National Food Chain Safety and Animal Health Directorate of Csongrád-Csanád County, Hungary. The procedures were performed according to the guidelines of the Scientific Committee of Animal Experimentation of the Hungarian Academy of Sciences (updated Law and Regulations on Animal Protection: 40/2013. (II. 14.) Gov. of Hungary), following the EU Directive 2010/63/EU on the protection of experimental animals, and in accordance with the ARRIVE guidelines[64].

Young adult, male Sprague-Dawley and Wistar rats (body weight: 250 g; n = 98) were used in these experiments. Animals were acquired from the Central Animal House of Biological Research Center, Szeged (Charles River Laboratories breed) and the animal house of the Department of Pharmacodynamics and Biopharmacy, University of Szeged (Charles River Laboratories breed). Standard rodent chow and tap water were supplied ad libitum. The animals were housed under constant temperature, humidity, and lighting conditions (23 °C, 12:12 h light/dark cycle, lights on at 7 a.m.).

2.2. Brain slice preparations

The brains of the rats were removed under deep anesthesia (4-5 % isoflurane in N_2O: O_2; 2:1). Coronal brain slices (350 μm) anterior to bregma were cut with a vibrating blade microtome (Leica VT1000S, Leica, Germany), and collected in ice-cold aCSF (composition of aCSF in mM concentrations: 130 NaCl, 3.5 KCl, 1 NaH_2PO_4, 24 $NaHCO_3$, 1 $CaCl_2$, 3 $MgSO_4$ and 10 D-glucose). Four to six slices were transferred to an incubation chamber filled with carbogenated aCSF (difference in composition in mM concentrations: 3 $CaCl_2$ and 1.5 $MgSO_4$) and kept at room temperature (~20-22°C). Individual slices were placed in an interface type recording tissue chamber (Brain Slice Chamber BSC1, Scientific Systems Design Inc., Ontario, Canada) and continuously perfused with carbogenated aCSF at a rate of 2.5 ml/min. Chamber temperature was kept at 32°C using a dedicated proportional temperature controller unit (PTC03, Scientific Systems Design Inc., Ontario, Canada)[61, 65].

2.3. Local field potential recordings

LFP filtered in DC mode (<1 Hz) was acquired via a glass capillary microelectrode (1-3 MΩ) filled with 150 mM NaCl and 1 mM HEPES. The microelectrode was inserted into the 3rd cortical layer (Fig. 4A), and an Ag/AgCl reference electrode was positioned in the recording chamber. The glass capillary microelectrode was connected to a custom-made dual-channel

electrometer (including AD549LH, Analog Devices, Norwood, MA, USA), and the signal was fed to dedicated differential amplifiers and associated filter modules (NL106 and NL125, NeuroLog System, Digitimer Ltd., United Kingdom). The recorded analogue signal was converted to digital signal and displayed live using an Acknowledge environment (MP 150, Biopac Systems, Inc) at a sampling frequency of 1 kHz[61].

2.4. Intrinsic optical signal imaging

For IOS imaging, slices were illuminated by a halogen lamp (Volpi AG, Intralux 5100, Schlieren, Switzerland). Image sequences were captured at 1 Hz with a monochrome charge-coupled device (CCD) camera (spatial resolution: 1024 × 1024 pixel, Pantera 1M30, DALSA, Gröbenzell, Germany) attached to a stereomicroscope (MZ12.5, Leica Microsystems, Wetzlar, Germany), yielding 6-10 x magnification. Image sequences were analyzed off-line; the area of the SD focus, the total area covered by the propagating SD, and the propagation velocity of SDs were analyzed after contrast enhancement in FIJI (ImageJ).

2.5. Comparative analysis of spreading depolarizations under osmotic or metabolic stress

2.5.1. Methods of SD elicitation

KCl injection

SDs were evoked by pressure injection of 1M KCl (40 ms, 30 psi, approximately 150 picoliter) via a glass micropipette, using a picospritzer (Picospritzer III, Parker Hannifin, Hollis, USA). The micropipette was lowered into the 3rd cortical layer at a distance of 500 μm from the recording electrode. Four-to-five successive SDs were initiated in each slice at 10-12 min intervals (n=38) (Fig. 4B$_1$).

*Electric stimulatio*n

In order to elicit SD with electric stimulation, a concentric bipolar needle electrode (WPI, Sarasota, FL, USA) was positioned onto brain slices, at a distance of approximately 800–1000 μm from the DC potential recording electrode. The elicitation of SD followed previously established principles[66]. The stimulating electrode was connected to an opto-coupled stimulus isolator with constant current output (NL 800, Digitimer Ltd., United Kingdom), a pulse generator (NL301), a width-delay panel (NL405), and a pulse buffer (NL510), which enabled the adjustment of the duration of the stimuli at will. Stimulation was implemented with single, cathodal constant current pulses. The charge delivered was increased stepwise until SD was initiated, quantified as Q [μC] = I [mA] x t [ms], and ranged between 50-100 μC. Four-to-five

consecutive SDs were initiated in each slice at 10-12 min intervals to allow full recovery between events (n=51) (Fig. 4B_1).

Hypo-osmotic challenge

Slices (n=31) were exposed to hypo-osmotic solutions which were prepared by reducing the NaCl concentration of aCSF from the regular 130 to 40-120 mM (HM_{40}-HM_{120}), while other components and the pH of the medium were unaltered. The results shown here were obtained with HM_{60} because this condition regularly evoked spontaneous SDs. Electrophysiological recording or IOS imaging was initiated during normal aCSF incubation, 10-15 min before switching to HM superfusion, and pursued 15-20 min into HM incubation (Fig. 4B_2). SD occurred spontaneously in response to osmotic stress.

Oxygen-glucose deprivation

OGD was induced by superfusion of glucose-free aCSF (glucose was substituted with sucrose at equimolar concentration) on slices (n=40), and the solution was gassed with 95 % N_2 + 5 % CO_2. Electrophysiological recording or IOS imaging was initiated during normal aCSF incubation, 10-15 min before OGD onset, and pursued for 15-20 min after OGD onset (Fig. 4B_2). OGD invariably gave rise to an SD event. In selected slices (n=5), aCSF incubation was resumed after OGD for 5 min, and OGD was imposed again for 30 min, to test whether a subsequent SD event could generate.

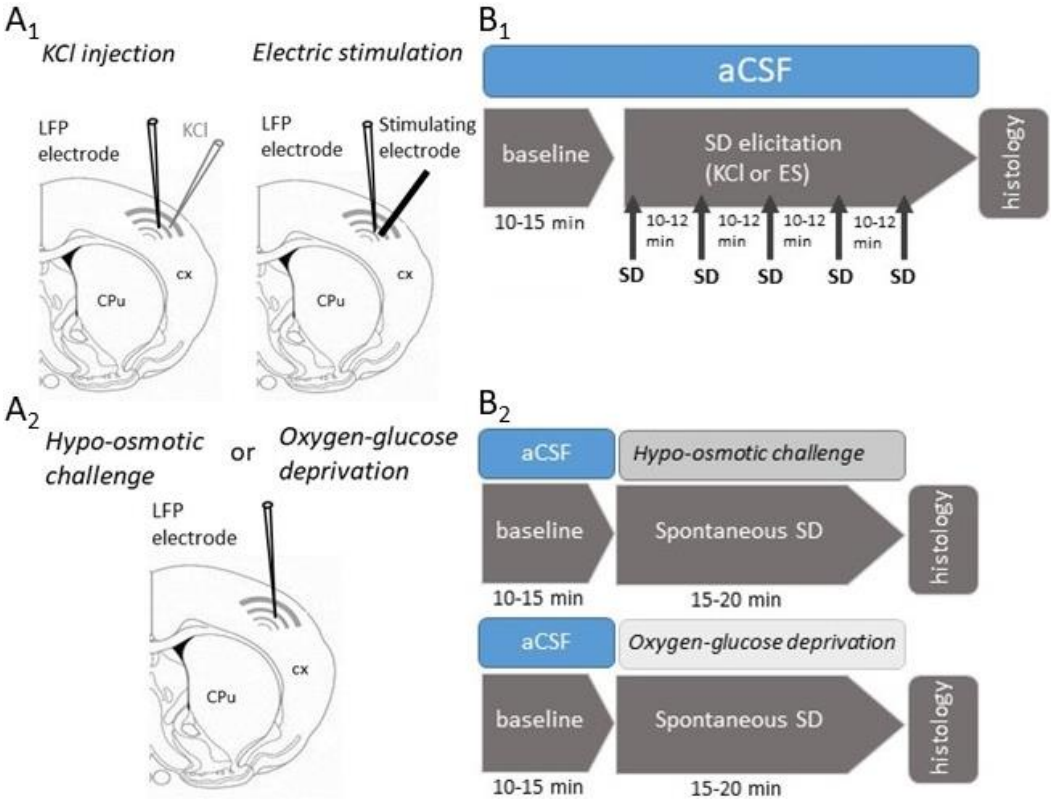

Figure 4. Graphical illustration of the experimental protocols. Schematic drawings of the preparations used for the experiments: **A1,** KCl injection (left), electric stimulation (right). **A2**, oxygen-glucose deprivation or hypo-osmotic challenge. Timelines show the phases of the experimental protocol: **B1**, Experimental protocol in KCl and ES groups; **B2**, Experimental protocol in HM and OGD groups. Abbreviations: aCSF; artificial cerebrospinal fluid, CPu; caudate putamen, cx; cerebral cortex, ES; electric stimulation, KCl; 1 M KCl microinjection, LFP; local field potential, SD; spreading depolarization.

2.5.2. Histology

TTC staining

The size of the lesion was determined by 2,3,5-triphenyltetrazolium chloride (TTC) staining. The brain slices (n=30) were incubated in a 2 % solution of TTC in 0.1 M phosphate buffered saline (PBS) for 20 minutes at room temperature. The sections were subsequently immersed and stored in 4 % paraformaldehyde for 24 h. The stained sections were then mounted on microscope slides and coverslipped with glycerol. Images were taken of the cortex with Nikon-DS Fi3 camera attached to a Leica DM 2000 Led light microscope (Leica Microsystems GmbH, Germany) at 10 x magnification.

Hematoxylin-eosin staining

For proper visualization of cell damage, representative TTC stained slices were rinsed with PBS and cryoprotected in 30 % sucrose in PBS. Coronal, 10-µm-thick frozen sections were cut with a freezing microtome (Leica CM 1860 UV, Leica, Germany). The sections were stained with hematoxylin (Sigma-Aldrich, USA) for 25 s, rinsed with distilled water, then stained with eosin

(Sigma-Aldrich, USA) for 15 s, rinsed with distilled water, dehydrated, and coverslipped with Eukit® (Merck, USA). The sections were examined with optical microscopy; photomicrographs at 40 x magnification were taken with a Nikon-DS Fi3 camera attached to a Leica DM 2000 Led light microscope (Leica Microsystems GmbH, Germany).

2.6. Observation of simultaneous depolarization on brain slices

2.6.1. Experimental protocols

Brain slices were exposed to hypo-osmotic challenge as described above. The results shown here were obtained with HM_{100} and HM_{60}. The use of HM_{60} was relevant for the pharmacological set of experiments (see: 2.6.2. Pharmacological treatments), because this condition regularly evoked spontaneous SDs to be modified by the drugs used (Fig. $5A_2$& Fig. $5B_1$). In HM treated slices, after a baseline period, aCSF was replaced with HM in the recording chamber as the experimental condition (n=57, HM_{100}: 16 slices, HM_{60}: 41 slices). Control slices were incubated in aCSF throughout the recording (n=21), the first SD (SD1) was elicited by electric stimulation, and a subsequent rSD was induced by transient anoxia (2.5 min) (Fig. $5A_1$). Hyper-osmotic solutions (HRM) contained additional mannitol in normal aCSF at 100 mM concentration (n=11). To evaluate the impact of HRM on the assessed variables, slices were incubated in HM first for 30 min, then HM was replaced with HRM. The SD1 occurred spontaneously in HM. A subsequent rSD was elicited by transient anoxia in HRM (Fig. $5A_3$).

2.6.2. Pharmacological treatments

Slices were randomly exposed to various pharmacological treatments. For edema reduction, the $Na^+/K^+/Cl^-$ cotransporter blocker Bumetanide (Bum, Sigma-Aldrich; 1 mM) and the AQP4 channel inhibitor TGN-020 (Tocris; 100 μM) were co-applied (n=16; Fig. $5B_1$). To inhibit swelling related glutamate efflux via VRAC, slices were exposed to the channel blocker DCPIB (Tocris; 20 μM) (n=21; Fig. $5B_1$). NMDA receptors were blocked by the non-competitive NMDA receptor antagonist MK-801 (Tocris; 100 μM), co-applied with the competitive α-amino-3-hydroxy-5-methyl-4-isoxazolepropionic acid (AMPA)/kainate receptor antagonist CNQX (Tocris; 20 μM) (n=13; Fig. $2B_1$). TFB-TBOA (Tocris; 10 μM and 100 μM) an EAAT inhibitor was washed on the slices to explore whether glutamate uptake was functional (n=4; Fig. $5B_2$). Finally, fluorocitrate (Sigma; 0.5- 1 mM), a drug that disrupts the citrate cycle in astrocytes was applied to paralyze astrocytes (n=7; Fig. $5B_2$)[67-71].

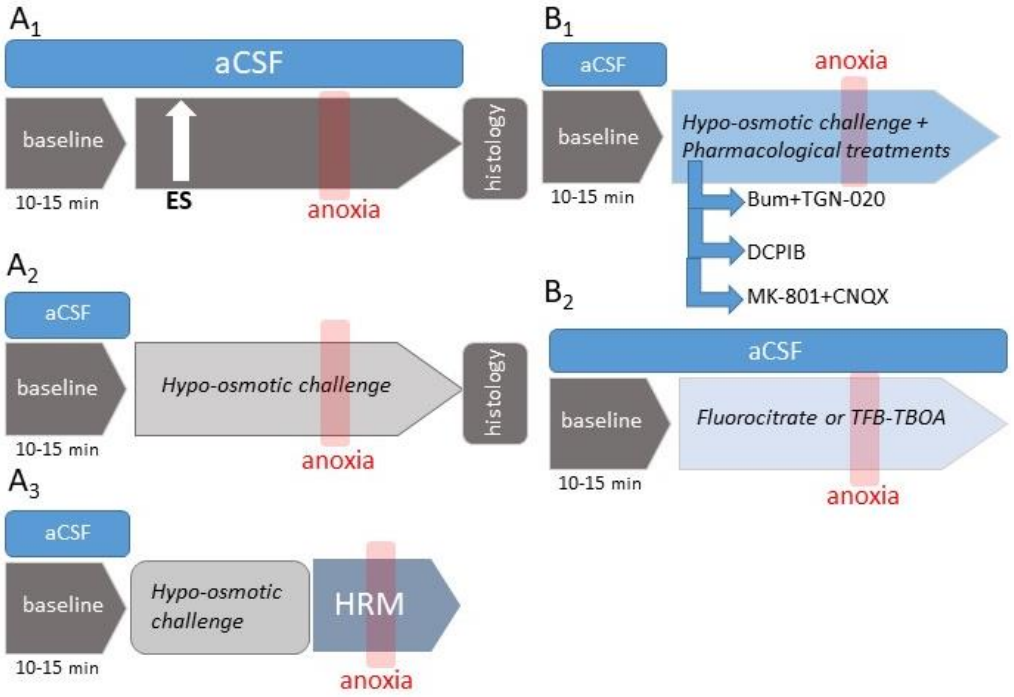

Figure 5. Illustration of the experimental protocols. Timelines show the phases of the experimental protocols: **A_1,** control condition; **A_2,** hypo-osmotic challenge; **A_3,** HRM treatment; **B_1,** hypo-osmotic challenge + pharmacological treatments; **B_2,** fluorocitrate or TFB-TBOA treatment. Abbreviations: aCSF; artificial cerebrospinal fluid, Bum; Bumetanide, ES; electric stimulation, HRM; hyper-osmotic medium.

2.6.3. Measurement of extra-synaptic glutamate concentration

Extra-synaptic glutamate concentrations were acquired using oxidase enzyme-based microelectrode biosensors (tip diameter: 30-40 µm) with constant potential amperometry[72]. Biosensors were constructed of Pt/Ir wires (Goodfellow, Huntington, UK), inserted into a pulled glass capillary (Harvard Apparatus, Edenbridge, UK). A poly-m-phenylenediamine (PPD) screening layer was deposited to the Pt/Ir surface by electropolymerization (20 min) with 700 mV constant potential. An encapsulated bio-layer containing glutamate oxidase was then deposited and fixed on the Pt/Ir surface. Biosensors were calibrated before and after the experiments in 0.01 M PBS with stepwise injections of glutamate concentration standards (5, 10, 15, 20, 25, 30, 35, 40, 45 µM). Glutamate oxidase enzyme sensitivity was confirmed by the application of 5 µM D-serine. During measurements, a constant potential of 500 mV was applied vs. an Ag/AgCl- electrode placed in the recording tissue chamber. Glutamate biosensor was lowered into the cortex together with LFP microelectrode and control sensor covered with bovine serum albumin (BSA, SigmaAldrich, St Quentin Fallavier, France) only. Control biosensors recorded negligible currents (glutamate independent) compared with glutamate biosensors. Biosensors were connected to a dedicated 3-electrode potentiostat (Quadstat)

equipped with an eDAQ data acquisition system (eDAQ Pty Ltd., Colorado Springs, CO, USA) and a dedicated eDAQ Chart program.

2.6.4. Histology

Golgi-Cox staining

To examine the morphology and swelling of astrocytes, a modified Golgi-Cox staining was used[73]. Brain slices were stained with FD Rapid GolgiStainTM Kit (FD Neurotechnologies, Inc., USA). The slices were postfixed in 4 % paraformaldehyde (PFA) containing 8 % glutaraldehyde for 24 h at room temperature. The sections were incubated in Golgi impregnation solution (equal volumes of solution A and solution B). Following impregnation, the brain slices were transferred into solution C and incubated at 4 °C for 24 h in dark. After the incubation in solution C, stained slices were dehydrated in solutions of increasing ethanol concentration (50 %, 70 % and 95 % and absolute ethanol), then mounted on microscope slides in 0.2 % polyvinyl-alcohol, and coverslipped with glycerol. Representative images were taken from 2nd-3rd cortical layer with Nikon-DS Fi3 camera attached to a Leica DM 2000 Led light microscope (Leica Microsystems GmbH, Germany).

Electron microscopy

For electron microscopic examination cross cortical blocks were dissected from representative brain slices. The samples were postfixed in 3 % glutaraldehyde and 2.25 % dextran in 0.1 M phosphate buffer (pH=7.4) for a week. Semi-thin sections were cut plane on an ultramicrotome (Ultracut E, Reichert-Jung) and stained on object glasses with toluidine blue. Ultrathin sections were cut from the same blocks and collected on copper slot grids. The preparations were contrasted with 5 % uranyl acetate and Reynolds lead citrate solution. The samples were analyzed with a Jeol JEM-1400 Plus transmission electron microscope, and photographs were taken with a CCD camera.

2.7. Data analysis

LFP traces were stored using a personal computer equipped with a dedicated software (AcqKnowledge 4.2 for MP 150, Biopac Systems, Inc., USA). Data analysis was conducted offline and was assisted by the inbuilt tools of AcqKnowledge 4.2 software.

To characterize SD events, the amplitude, the slope of depolarization and repolarization, and the duration of SD were quantitated in the LFP traces filtered in DC mode. These variables are conventionally taken as a measure of the propensity of the tissue to bear SD (e.g. slower depolarization or smaller amplitude disclose lower SD susceptibility)[74-76], and to predict the injurious potential of SD (the duration of SD or the cumulative duration of recurrent SDs

correlate with the degree of ischemic injury)[7, 16]. The duration of SD may also disclose the severity of the ongoing injurious condition. As such, SD becomes remarkably prolonged or terminal when the metabolic crisis in the tissue is severe[3].

In the IOS image sequences, several spatial features of SD/SiD events were measured after background subtraction and inbuilt automatic or manual thresholding in FIJI, and expressed relative to the full surface area of the cortex in the brain slice. First, the focal area of each event was estimated. Next, the area of sustained IOS intensity elevation following SD1 was expressed. Finally, the maximal cortical area covered by SD1 propagation or SiD were measured. The calculation of the propagation velocity was aided by the IOS signal and was more accurate than relying on LFP recordings, due to the perceptible direction of SD propagation.

SD events with amplitude < 3 mV or those where the post-SD DC signal remained level were excluded from data analysis.

Slice swelling over the experimental protocol was quantitatively evaluated by the change in the surface area of the full slice relative to baseline, at a temporal resolution of 1/100 s, and depicted in temporal correspondence with IOS variations at two ROIs. Slice area measurements were performed after contrast enhancement in FIJI.

The excitability of the nervous tissue was characterized with the amplitude of evoked field potentials, and the electric threshold of SD elicitation. For the latter, the charge delivered was calculated as Q[μC]=I[mA] x t[ms], and it was raised stepwise with an interstimulus interval of 2 min until SD was observed. The threshold of SD elicitation was illustrated on a logarithmic scale.

After binary conversion, TTC stained images were manually thresholded, particles were measured with the inbuilt “analyze particles” function of FIJI and expressed as % area relative to baseline.

Images of Golgi-Cox-stained astrocytes were processed after auto leveling and background correction in FIJI. Cellular swelling was measured after binary conversion and manual thresholding using the embedded Otsu filter in FIJI. Astrocyte soma areas were outlined, then the outlined area was measured automatically using the “analyze particles” function in FIJI. Finally, the swelling was expressed as area change relative to the mean area in the control group.

Quantitative data are given as mean±standard deviation (stdev). Statistical analysis was conducted with the software SigmaPlot 13.0 (Systat Software, Inc. San Jose, USA). Data sets were evaluated first with a Shapiro-Wilk test of normality. For data sets with normal distribution, a two-tailed T-test or one-way analysis of variance (ANOVA) were used, followed

by a Holm-Sidak post hoc test when appropriate. Correlation analysis was conducted with a one-tailed Pearson correlation test. Levels of significance were set at $p<0.05$* or $p<0.01$**. Distinct statistical methods are provided in each Figure legend in detail.

3. Results

3.1. Comparative analysis of spreading depolarizations under osmotic or metabolic stress

3.1.1. Prolonged SDs occur upon acute osmotic stress and in response to oxygen-glucose deprivation

First, we compared the electrophysiological features of spontaneous SDs occurring in hypo-osmotic medium or during oxygen-glucose deprivation to SDs evoked in aCSF. Prolonged SDs and incomplete DC potential recovery were observed during OGD incubation and HM exposure compared to SDs evoked by KCl or ES in aCSF (195.65±117.05 vs. 112.14±88.39 vs. 33.95±26.615 vs. 54.75±26.72 s, HM vs. OGD vs. KCl vs. ES) (Fig. 6B&D). The incomplete DC potential recovery from SD was also reflected by the reduced slope of repolarization in the HM and OGD groups compared to aCSF (0.30±0.17 vs. 0.12±0.10 vs. 0.45±0.27 vs. 0.50±0.24 mV/s HM vs. OGD vs. KCl vs. ES) (Fig. 6E). On the other hand, the greatest SD amplitudes were measured during HM exposure and ES (-17.59±5.3 vs. -7.64±5.33 vs. -7.09±3.4 vs. -15.03±5.01 mV, HM vs. OGD vs. KCl vs. ES) (Fig. 6C).

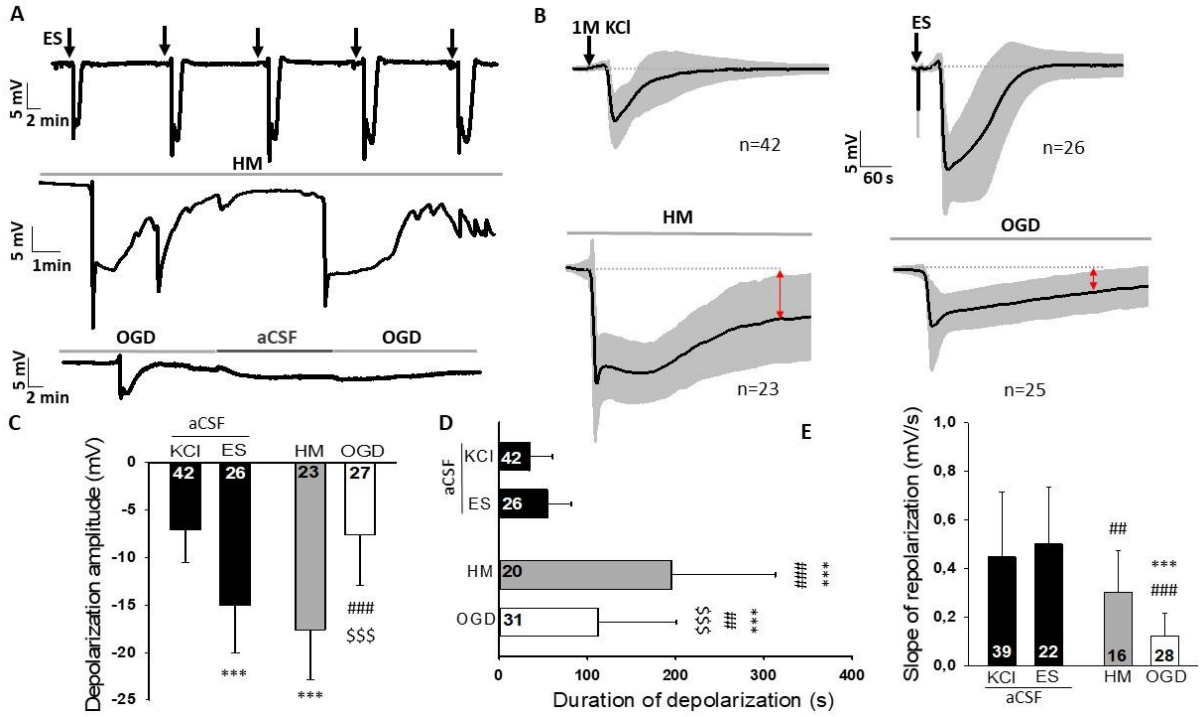

Figure 6. The electrophysiological characterization of spreading depolarizations. A, Representative DC potential recordings demonstrate the experimental protocols. Slices were exposed to aCSF (SD initiation here: ES), HM or OGD. Black vertical arrows indicate ES in aCSF, grey horizontal timelines depict the exposure to the experimental condition (HM or OGD). **B,** The SD-related negative DC shifts (mean±stdev) for each experimental group. Black vertical arrows indicate KCl application or ES in aCSF, grey horizontal timelines depict the exposure to the experimental condition (HM or OGD). Red arrows highlight incomplete repolarization relative to pre-SD baseline. **C,** The maximum amplitude of SD. **D,** The duration of SD. **E,** The slope of repolarization. Data are given as mean±stdev. Sample size (i.e. number of SD events analyzed) is indicated in each bar. One-way analysis of variance (ANOVA) followed by a Holm-Sidak post hoc test was used for statistical analysis. The level of significance is given as $p<0.001$*** vs. KCl; $p<0.01^{\#\#}$ and $p<0.001^{\#\#\#}$ vs. ES; $p<0.001^{\$\$\$}$ vs. HM. Abbreviations; aCSF; artificial cerebrospinal fluid, ES: bipolar electric field stimulation, KCl: microinjection of 1M KCl solution, HM: hypo-osmotic medium, OGD: oxygen-glucose deprivation.

3.1.2. Severe osmotic stress and oxygen glucose deprivation enhance the area invaded by SD

Next, we set out to explore whether longer SDs also invade larger tissue area, indicative of a larger bulk of tissue at risk of injury. To address this question, we performed IOS imaging of the brain slices. IOS imaging was also suitable to calculate the rate of SD propagation and SD latency (i.e. the time between the onset of HM or OGD incubation and the appearance of the SD focus).

The SD latency with respect to the onset of treatment was much longer in slices exposed to HM than to OGD (549.1±164.59 vs. 165.75±52.3 s, HM vs. OGD) (Fig. 7E), while SD occurred

within seconds after KCl or ES elicitation in aCSF. SDs during HM or OGD exposure propagated at a higher rate than SDs induced by KCl or ES in aCSF (4.24±1.32 vs. 2.15±0.83 vs. 1.7±0.59 vs. 1.94±0.73 vs. mm/min, HM vs. OGD vs. KCl vs. ES) (Fig. 7C).

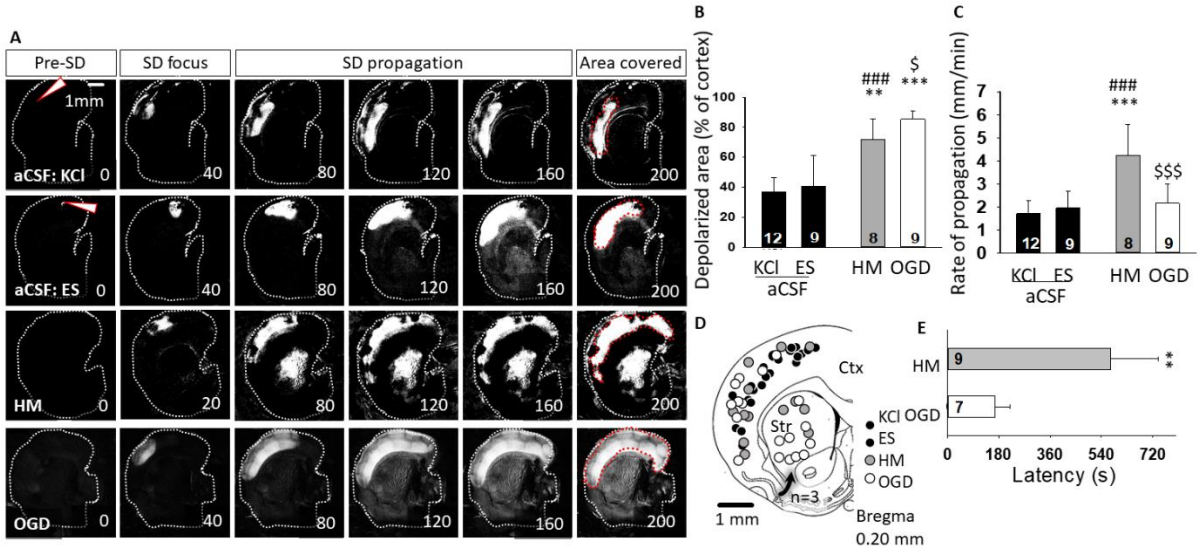

Figure 7. Intrinsic optical signal (IOS) imaging of spreading depolarizations. A, Background subtracted IOS image sequences demonstrate SD evolution. Increased IOS intensity indicates SD. White arrowheads show the position of the KCl filled microcapillary or the stimulating electrode in the aCSF condition. Red dotted lines in "Area covered" delineate the maximal cortical area invaded by the SD. **B,** The cortical area covered by SD relative to the total surface of the cortex. **C,** The rate of SD propagation. **D,** The localization of all SD foci observed in the cerebral cortex (Ctx) and in the striatum (Str) in a schematic drawing. Some of the cortical SDs (n=3) invaded the striatum at the ventral tip of the cortex, which is shown by the arrow. **E,** The latency of spontaneous SDs with respect to HM or OGD exposure. Data are given as mean±stdev. Number of SD events analyzed is indicated in each bar. ANOVA followed by a Holm-Sidak post hoc test (B, C) or a two-tailed T-test (E) was used for statistical analysis. The level of significance is given as $p<0.001$*** vs. KCl; $p<0.01^{\#\#}$ and $p<0.001^{\#\#\#}$ vs. ES; $p<0.05^{\$}$, $p<0.01^{\$\$}$ and $p<0.001^{\$\$\$}$ vs. HM. Abbreviations: aCSF; artificial cerebrospinal fluid, ES; bipolar electric field stimulation, KCl; microinjection of 1M KCl solution, HM; hypo-osmotic medium, OGD; oxygen-glucose deprivation, Str; striatum, Ctx; cerebral cortex.

The tissue area representing the SD focus was enlarged during HM or OGD incubation compared to ES or KCl-evoked SDs in aCSF (2.64±1.27 vs. 2.23±0.82 vs. 1.37±0.5 vs. 1.93±0.74 % of the total cortical area, HM vs. OGD vs. KCl vs. ES) (Fig. 7A). SDs also invaded a significantly larger cortical area in the HM and in the OGD conditions compared to aCSF (71.98±13.43 vs. 85.32±5.32 vs. 36.72±9.39 vs. 40.4±20.66 % of total cortical area, HM vs. OGD vs. KCl vs. ES) (Fig. 7A&B). SDs initiated with a focal stimulus (KCl and ES) obviously evolved at the site of trigger delivery. During HM treatment or OGD, depolarization foci occurred in the parietal and temporal cortex (Fig. 7D).

Furthermore, SDs also occurred in the striatum during OGD in all slices examined (n=9) (Fig. 7A&D). In HM, SD emerged in the striatum in 4 of 9 slices, and cortical SDs invaded the striatum from the ventral tip of the cortex in an additional 3 slices (Fig. 7D). The SDs with a striatal focus occurred invariably after the cortical SDs in these experiments, with a latency of 0.5-2 min with respect to the generation of the cortical SDs (34.85±7.21 and 137.89±59.39 s HM and OGD).

3.1.3. Oxygen-glucose deprivation and osmotic stress restrain cell survival after SD

Finally, we moved on to analyze the histological outcome of SDs. TTC staining commonly used for the detection of lesion development[77-79] was applied to quantify the SD-related tissue injury. We accepted higher numbers of TTC-positive cellular compartments (i.e. particles) to indicate better tissue viability[53]. The SD-related TTC-positive particle loss was obvious after a single SD in HM or OGD (26.45±10.64 and 11.44±6.42 vs. 54.33±21.21 per 1000 μm^2, HM and OGD vs. KCl) (Fig. 8A&B). Also, the repeated elicitation of SD with ES in aCSF caused a significant reduction in particle number (30.28±9.84 vs. 54.33±21.21 per 1000 μm^2, ES vs. KCl) (Fig. 8A&B). Corresponding neuronal injury was observed in hematoxylin-eosin-stained sections: condensed, fragmented nuclei and vacuolization indicated pronounced neuronal damage after OGD and HM treatment (Fig. 8A). This was also seen to a lesser degree after recurrent SDs triggered with ES. In contrast, neurons were preserved and had a large, round nucleus with a prominent nucleolus after repeated, KCl-evoked SDs (Fig. 8A). Finally, a linear negative correlation was found between the number of TTC-positive particles and the size of the cortical area engaged by SD (Fig. 8C).

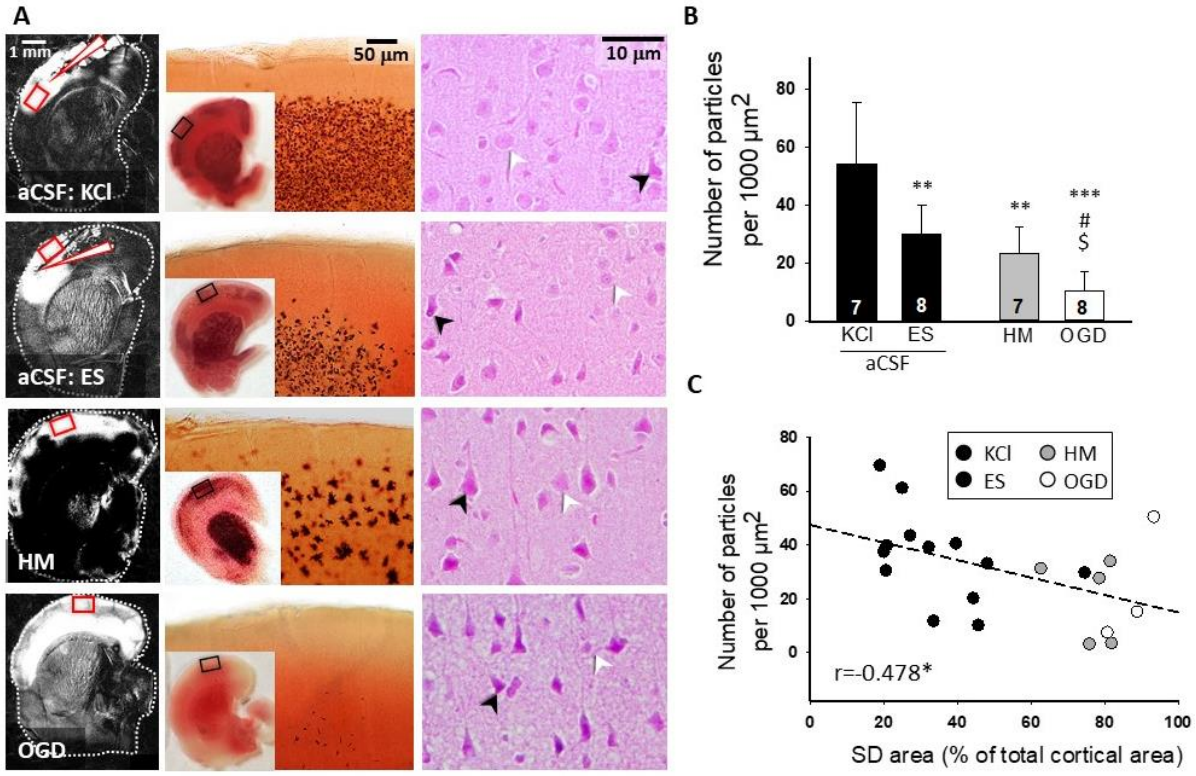

Figure 8. Histological analysis of SD-related tissue injury. A, Representative background subtracted IOS images to the left show the surface of the cortex covered by the propagating SD (bright region). White arrowheads are pointing at the position of the site of SD elicitation with KCl or ES. In the middle, representative light microscopic images of brain slices stained with TTC after the passage of SDs (4-4 SDs were elicited in each slice with KCl or ES; a single SD occurred in response to HM or OGD) show macroscopic injury. Representative photomicrographs of hematoxylin-eosin-stained sections to the right demonstrate neuronal injury. Black arrowheads indicate injured neurons; white arrowheads show viable cells with intact nuclei in the somatosensory cortex. **B,** The number of TTC-stained cellular compartments (i.e. particles). **C,** Correlation between the number of particles and the cortical area bearing an SD. Data are given as mean±stdev. Sample size (i.e. number of slices analyzed) is indicated in each bar. Statistical analysis relied on one-way analysis of variance (ANOVA) followed by a Holm-Sidak post hoc test (B), or one-tailed Pearson correlation analysis (C). The level of significance is given as $p<0.05$* and $p<0.01$** vs. KCl; $p<0.01$ ## and $p<0.001$ ### vs. ES; $p<0.05$ $ vs. HM. Abbreviations: aCSF; artificial cerebrospinal fluid, ES; bipolar electric field stimulation, KCl; microinjection of 1M KCl solution, HM; hypo-osmotic medium, OGD; oxygen-glucose deprivation.

3.2. Observation of simultaneous depolarization on brain slices

3.2.1. Hypo-osmotic stress favors the evolution of SiD

To test the hypothesis that acute tissue swelling expands SD focus, we created extreme hypo-osmotic stress on brain slice preparations. SD1 occurred spontaneously during HM incubation or was elicited by electrical stimulation in normal aCSF (Fig. 9). Anoxia caused propagating rSD under aCSF incubation (Fig. 9A), but induced SiD predominantly in HM (35 of 44 slices, 80%) (Fig. 9B&D).

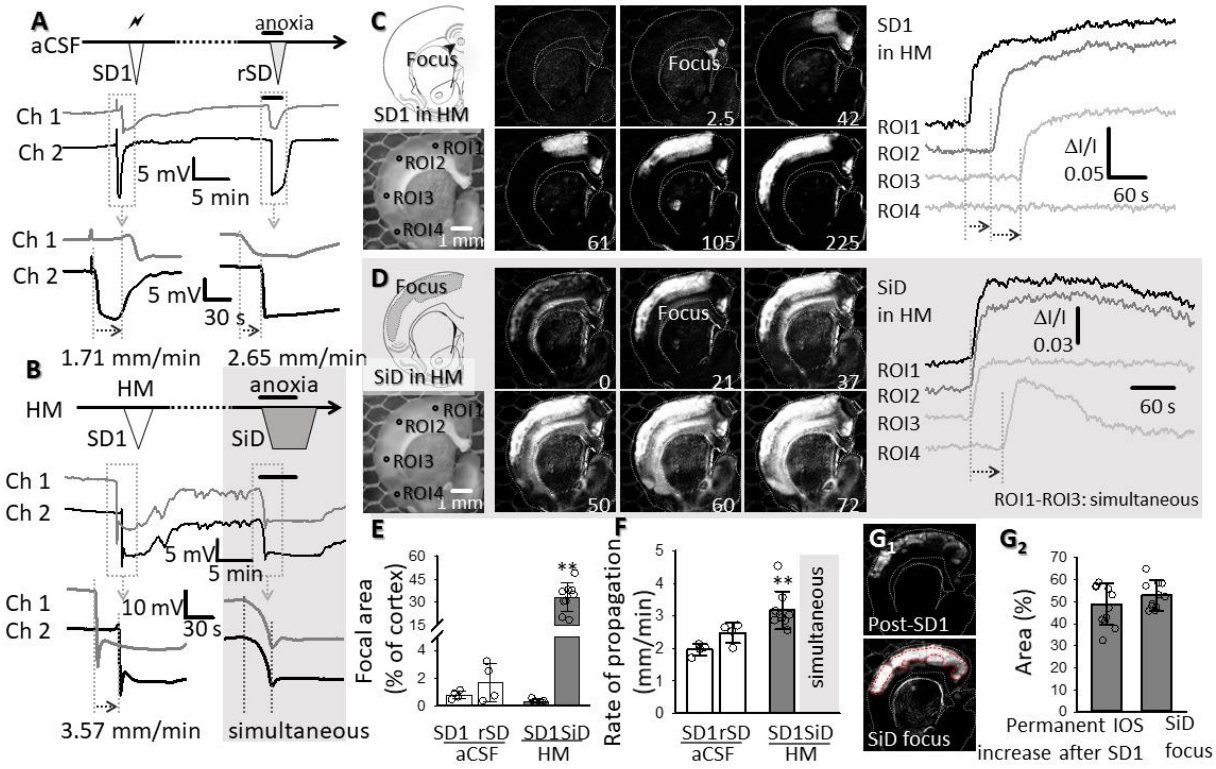

Figure 9. SD and SiD during osmotic stress in coronal brain slice preparations. A, The regular spreading nature of both SD1 and rSD in normal aCSF is shown in a representative electrophysiology experiment. SD1 was elicited by electrical stimulation and rSD was induced by transient anoxia (oxygen withdrawal of 2.5 min). **B,** SD1 occurred spontaneously to HM exposure (HM_{60} here), while the subsequent event was induced 15 min later by transient anoxia. The original electrophysiological recordings demonstrate that SD1 was a spreading event, followed by an SiD in response to anoxia. **C and D,** In background subtracted IOS images of a HM-incubated brain slice, the temporal characteristics of SD1 in Panel C reveal a punctual focus and propagation in the upper cortical layers. In Panel D, subsequent anoxia in HM (HM_{100} here) induced SiD of an extensive bulk of cortical tissue (ROI1-ROI3; SiD), and the propagation of the event towards the ventral tips of the cortex (ROI3→ROI4). Note the simultaneous increase of signal intensity (Panel D) at ROI1-ROI3, and the delay at ROI4 with respect to ROI1. **E,** The relative size of the focal area of SD/SiD measured in IOS images. **F,** The rate of propagation of depolarization events. **G,** The focal area of SiD incorporated the tissue zone characterized by sustained IOS intensity elevation following SD1. Images in G_1 were taken prior to SiD (post-SD1), and at the emergence of SiD (SiD focus). A red broken line delineates the post-SD1 high IOS intensity zone (the later SiD focus). The mean size of the tissue area is given in G_2 relative to the full size of the cortex. In Panels E-G, data are given as mean±stdev, individual values are shown with a dot plot. A Shapiro-Wilk test of normality indicated non-normal distribution for Panels E & F (p=0.050*), and normal distribution for Panel G_2 (p=0.304). Accordingly, data in Panels E & F were analyzed with a non-parametric Kruskal-Wallis test, followed by a Dunn post hoc analysis (E, p<0.01** vs. SD1 in HM; F, p<0.01** vs. SD1 in aCSF). Abbreviations: aCSF; artificial cerebrospinal fluid, SD1; first spreading depolarization, rSD; recurrent SD, SiD; simultaneous depolarization, HM; hypo-osmotic medium, ROI; region of interest.

IOS recordings revealed that the focus of SD1 was punctual (<1 % of total cortical area) in both aCSF and HM, and was localized to the upper layers of the dorsal-dorsolateral parietal cortex (Fig. 9C&E). SD1 propagated with a higher rate in HM than in aCSF (3.17±0.58 vs. 1.97±0.18 mm/min, HM vs. aCSF) (Fig. 9F). Anoxia in HM gave rise to SiD in 11 of 16 slices, implicating a sizeable area of the cortex (>50% of the total cortical area), which incorporated much of the tissue previously involved in SD1 propagation (Fig. 9D&G). In addition to the upper cortex, SiD progressively engaged the underlying deeper layers of the cortex (Fig. 9D). Collectively, these data show that under osmotic stress, the tissue engaged in the propagation of SD1 later turned into a sizeable depolarization focus identified as SiD. The elevated IOS intensity sustained after SD1 (Fig. $9G_1$&G_2) and the concomitant failure of complete repolarization from SD1 together predicted SiD occurrence.

In a few cases (n=3) after the spontaneous SD1 the subsequent simultaneous depolarization also occurred spontaneously, cancelling the need for the anoxic initiation of SiD. Note that the evolution of spontaneous SiD was similar to that of SiD triggered with transient anoxia in other slices (Fig. 10A). Repolarization after SD1 in HM was substantially delayed or incomplete. Further, small amplitude, irregular field oscillations evolved in synchrony on the DC potential trace. These field oscillations predicted the later SiD (Fig. 10B).

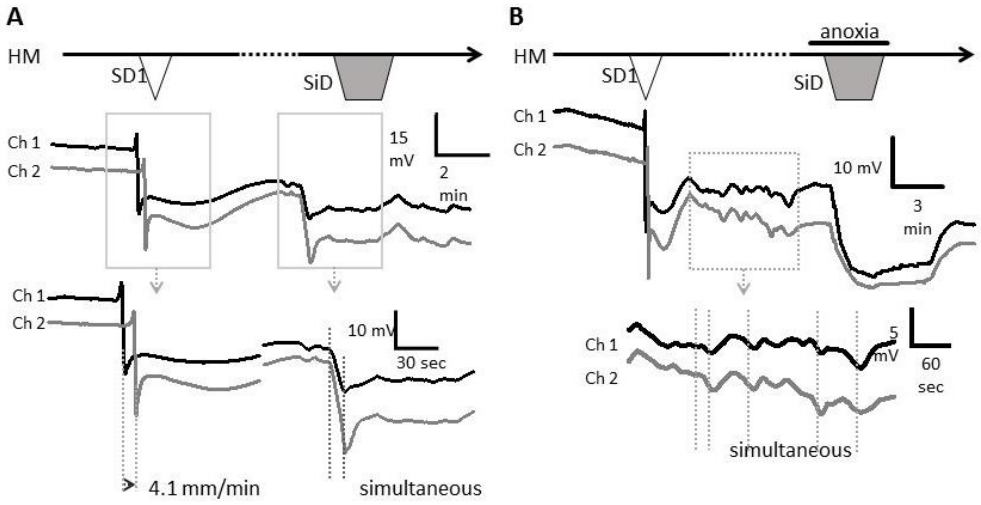

Figure 10. Direct current potential traces of spontaneously occurring SiD and simultaneous field oscillations. A, Spontaneously occurring SD1 and subsequent SiD. **B,** The repolarization phase of SD1 was incomplete, and small amplitude, irregular field oscillations evolved in synchrony on the two channels. This pattern of the DC signal was typical in case SiD ensued. Abbreviations: SD1; first spreading depolarization, SiD; simultaneous depolarization, HM; hypo-osmotic medium.

In 5 of 16 slices, typically 3-4, spatially distinct, punctual SD foci emerged in temporal synchrony (cumulative focal area < 3 % of total cortical area) in response to anoxia, to give rise to propagating SD waves, which ultimately fused. We identified these events as rSD with multifocal origin, and multifocal rSD was considered as a transition between classic rSD (i.e. single focus) and SiD (Fig.11).

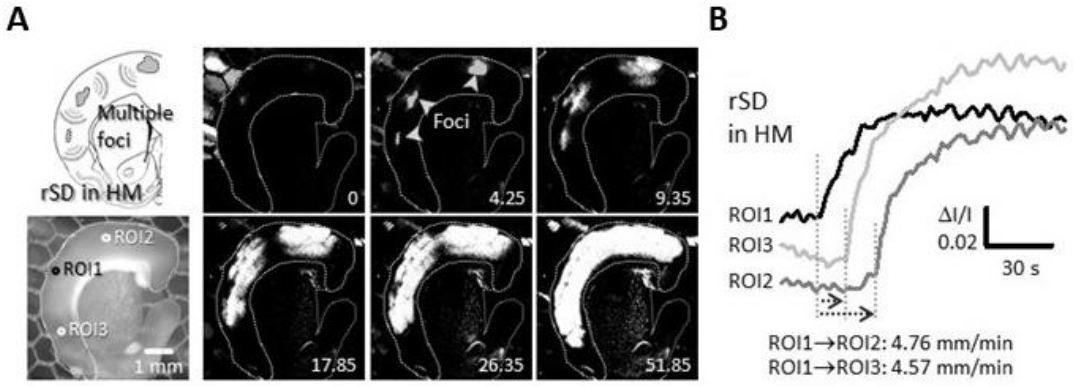

Figure 11. Intrinsic optical signal imaging of multifocal rSD. A, Representative images of a recurrent spreading depolarization (rSD) triggered with transient anoxia in brain slice preparation exposed to hypo-osmotic medium (HM_{100}). Note that the event propagated from three foci, attesting a multi-focal origin. **B,** Intrinsic optical signal intensity changes at three regions of interest (ROI1-3) placed between the foci demonstrated the propagation of the rSD. Images were obtained by template matching (movement artefact correction), background subtraction, smoothing and contrast enhancement. The temporal resolution of the image sequences is given in the lower right corner in seconds. Abbreviations: rSD; recurrent SD, HM; hypo-osmotic medium, ROI; region of interest.

3.2.2. Astrocyte swelling is implicated in SiD

To further explore the hypothesis that tissue swelling predisposes the tissue to SiD, we evaluated the degree of tissue swelling caused by the osmotic stress. The increase of the brain slice area was most conspicuous with the second depolarization event, rSD in aCSF and SiD in HM (Fig. $12A_{1-2}$). Under aCSF, slice surface area increased slightly with SD1 (with 1.09±0.68 pp.) and returned to baseline within minutes after SD1 (0.19±0.15 pp.). The maximum increase of the slice area was greater with rSD than with SD1 (4.75±1.33 vs. 1.09±0.68 pp., rSD vs. SD1), but the swelling was again transient and reversible (Fig. $12A_3$). In HM, slice swelling commenced upon HM exposure, and the slice area gradually increased to reach a considerable expansion already before SD1 (4.59±1.14 and 4.15±1.11 vs. 0.07±0.09 pp., HM_{60} and HM_{100} vs. aCSF) (Fig. $12A_4$). SD1 in HM occurred then spontaneously, and increased slice area with an additional, small extent (6.9±2.6 and 5.94±2 pp., HM_{60} and HM_{100}). The slice area showed negligible variations afterwards, with no recovery to pre-SD1 level (Fig. $12A_4$). It is important

that slice swelling preceded SD1 and SiD in HM, in contrast with aCSF, in which slice swelling was associated with SD1 and rSD.

Next, since astrocytes rapidly swell in response to hypo-osmotic stress, we hypothesized the pivotal role of astroglial edema in our HM model[26]. Astrocytes appeared clearly swollen in Golgi-Cox-stained slices and electron microscopic preparations after exposure to HM, especially after the passage of SD1 (Fig. 12B), substantiated by the quantitative evaluation of astrocyte soma area in the Golgi-Cox-stained sections (Fig. $12B_2$). In the electron microscopic images, both the perinuclear cytoplasm and astrocyte processes increased in size. The astrocyte cytoplasm displayed decreased electron density indicative of cellular edema, particularly after SD1 had been superimposed on the osmotic stress (Fig. $12B_3$).

Consequently, we posited further that swollen astrocytes must substantially contribute to SiD, because astrocyte swelling increases neuronal excitability[80]. The amplitude of evoked potential (EVP) was measured in the cerebral cortex was significantly greater in HM (171.0±11.8 and 184.3±7.4 vs. 93.1±9.3 μV, HM_{60} and HM_{100} vs. aCSF) (Fig. 12C). The latency of SiD occurrence to anoxia onset decreased markedly in HM (46.9±24.3 and 45.9±18.2 vs. 86.9±28.7 s; SiD in HM_{60} and HM_{100} vs. rSD in aCSF) (Fig. 12D). Likewise, the electric threshold of SD elicitation was drastically reduced in HM (50.1±15.7 and 52.5±18.4 vs. 1214.3±470.6 μC, HM_{60} and HM_{100} vs. aCSF) (Fig. 12E). In the latter set of experiments, the implication of astrocyte swelling was confirmed by repeating the SD threshold measurements with the addition of fluorocitrate to the aCSF, which decreased SD threshold similar to HM (51.0±22.9 and 52.5±18.4 μC, fluorocitrate and HM_{100}) (Fig. 12E).

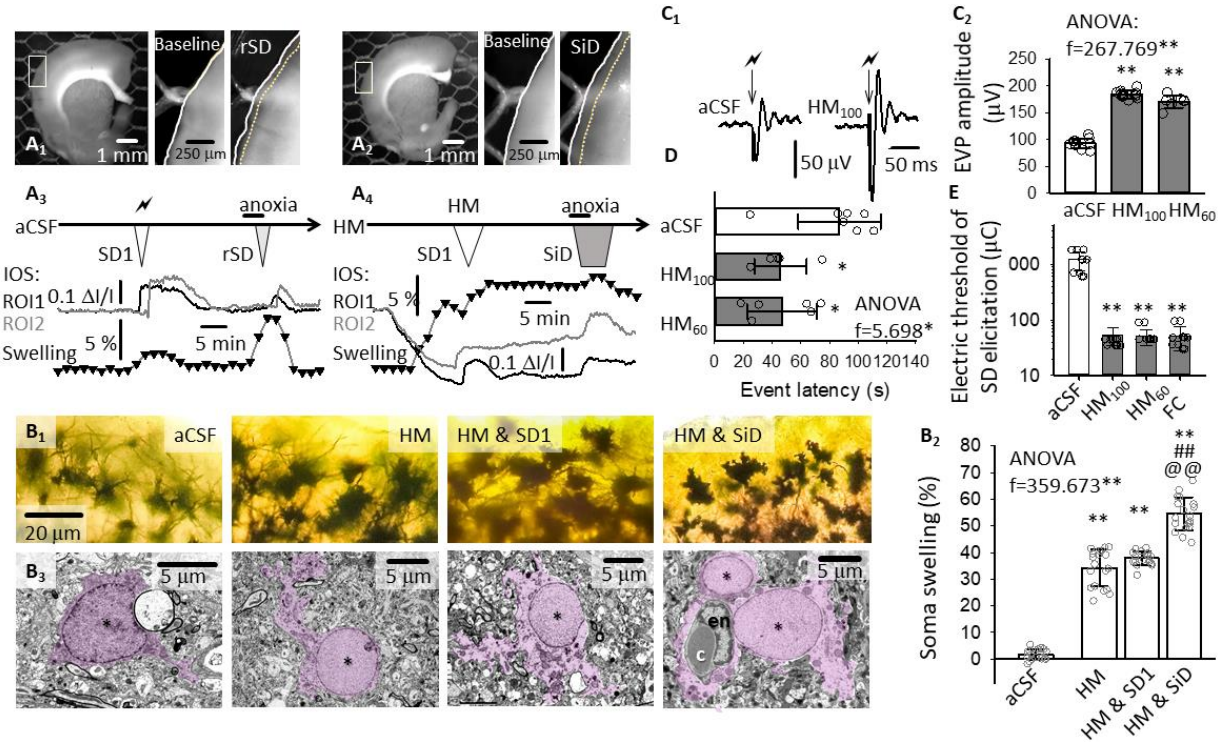

Figure 12. The implication of tissue edema and astrocyte swelling in SiD evolution. A, IOS images demonstrate slice swelling with rSD in normal aCSF (A_1), and with SiD in HM (A_2), represented by the displacement of the contour of the parieto-temporal cortex (inserts). Swelling over the experimental protocol was characterized by the change in the surface area of the full slice relative to baseline, at a temporal resolution of 1/100 s (trace with black triangles), and depicted in temporal correspondence with IOS variations at two ROIs (aCSF: A_3; HM: A_4). **B,** Golgi-Cox-stained sections (B_1) and electron photomicrographs (B_3) of astrocytes in aCSF, after SD1 in HM and after SiD in HM (asterisk: astrocyte nucleus; purple shading astrocyte cytoplasm and nucleus, c: capillary lumen filled with an erythrocyte). The soma swelling of astrocytes was measured in Golgi-Cox-stained preparations, and have been expressed relative to soma size in aCSF (B_2). **C,** The excitability of the nervous tissue. The amplitude of evoked potentials (EVP) was twice as great in HM compared to aCSF, as shown in representative recordings (C_1) and a quantitative bar chart (C_2). **D,** Latency of rSD in aCSF and SiD in HM after anoxia. **E,** The electric threshold of SD elicitation under aCSF, HM or fluorocitrate (FC) incubation. Data in Panels B_2, C_2, D and E are given as mean±stdev. Dot plots depict individual values in B_2, C_2, and D. Normal distribution of data was confirmed by a Shapiro-Wilk test (B_2, p=0.675; C_2, p=0.585; D, p=0.146; E, p=0.05*). Further statistical analysis was achieved with a one-way ANOVA ($p<0.05$* and $p<0.01$**), and a Sidak post hoc test ($p<0.05$* and $p<0.01$** vs. aCSF; in B_2, $p<0.01^{\#\#}$ vs. HM, $p<0.01^{@@}$ vs. HM & SD1), or a Kruskal Wallis test followed by a Dunn's post hoc test (E, $p<0.01$** vs. aCSF). Abbreviations: aCSF; artificial cerebrospinal fluid, SD1; first spreading depolarization, rSD; recurrent SD, SiD; simultaneous depolarization, HM; hypo-osmotic medium; IOS; intrinsic optical signal, ROI; region of interest, FC; fluorocitrate, EVP; evoked potential.

3.2.3. SiD evolution promotes lesion maturation

SD has been proposed to recruit viable ischemic penumbra tissue into the infarcted core[13]. Further, persistent cytotoxic edema has been implicated in the SD related dendritic injury[33]. Given this context, we hypothesized that astroglial swelling and the related SiD must have represented the actual tissue infarction in progress. We observed that the maximum depolarized tissue area engaged in SiD was invariably greater than the tissue area traversed by SD1 (76.8±11.4 vs. 60.9±10.7 %, SiD vs. SD1) (Fig. 13A& C). Macroscopic tissue damage assessed with TTC staining was obvious after SiD compared to SD1 in HM, or aCSF (Fig. 13B). The number of TTC-positive cellular compartments (i.e. "particles") was clearly reduced after SiD compared to SD1 in HM, or aCSF (5.0±1.1 vs. 35.8±3.0 vs. 43.5±1.0 particles per 1000 μm^2, SiD in HM vs. SD1 in HM vs. aCSF) (Fig. 13D). These results suggest that astrocytic edema and the linked SiD seriously jeopardize the survival of neurons and astrocytes. Malignant astrocyte swelling and impaired glutamate clearance drive the expansion of injurious spreading depolarization foci and impose significant damage to the nervous tissue.

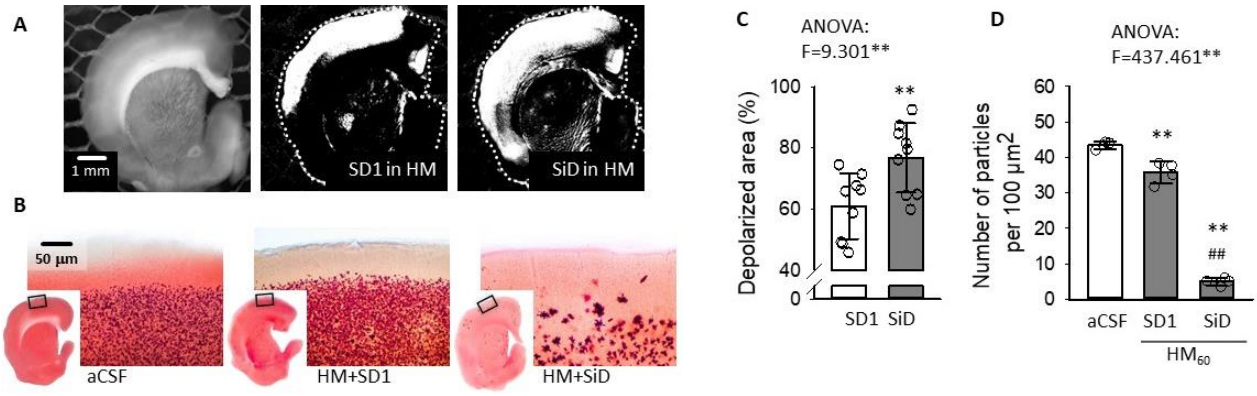

Figure 13. Cellular injury as a consequence of SD or SiD. A, The area covered by SD1 and the subsequent SiD as shown in representative background subtracted IOS images. **B,** TTC staining of brain slices after SD1 in aCSF, HM, and SiD in HM. **C,** Quantitative evaluation of the total area covered by SD1 and SiD. **D,** The number of TTC-stained particles after depolarization events. Data in C and D are given as mean±stdev; additional dot plots show individual values. After the evaluation of normal distribution with a Shapiro-Wilk test (C, p=0.077; D, p=0.616), statistical analysis relied on a one-way ANOVA in Panels C & D, p<0.01**, followed by a Sidak post hoc test (C: p<0.01** vs. SD1; D: p<0.01** vs. aCSF, p<0.01$^{\#\#}$ vs. SD1 in HM). Abbreviations: aCSF; artificial cerebrospinal fluid, SD1; first spreading depolarization, SiD; simultaneous depolarization, HM; hypo-osmotic medium.

3.2.4. Inhibition of astrocyte swelling or volume regulated glutamate release alleviates tissue edema and prevents SiD

Next, we set out to understand the underlying mechanisms of SiD by attempting to prevent it by pharmacological means. Edema-related glutamate release or impaired glutamate clearance

emerged as the most likely candidates to promote SiD, because astrocytes have been shown to swell and release glutamate in response to osmotic stress and SD[81-83]. To test this notion, extracellular glutamate concentration concomitant with slice swelling in HM was measured.

Extracellular glutamate gradually accumulated with slice swelling, to exceed 10 μM concentration by the time SD1 occurred. SD1 was associated with a glutamate peak followed by partially recovery. Then extracellular glutamate concentration remained constantly elevated above 15 μM, coincident with ongoing slice swelling. SiD caused a second glutamate peak with no recovery (>20 μM post-SiD) against a background of marked edema (Fig. 14A & C).

Inhibition of astrocyte AQP4 channels and NKCCs by TGN+Bum, or VRACs by DCPIB effectively reduced slice swelling related to HM exposure and SD (Fig. 14B). Furthermore, TGN+Bum or DCPIB profoundly diminished extracellular glutamate accumulation with SD1, and improved the glutamate recovery after anoxia (Fig. 14C & D). Furthermore, both treatments decreased the likelihood of SiD evolution significantly (2 of 16 (13%) vs. 3 of 23 (13%) vs. 28 of 33 (85%) slices; TGN+Bum vs. DCPIB vs. HM_{60}). Instead, the majority of the treated slices gave rise to rSD in response to anoxia. This was reflected in the size of the focal area of depolarization events. While the SD1 focus was punctual and very small (<1 % of the cortical surface) in all groups (Fig. 14E), the focus of SiD in the HM_{60} group engaged 55.5±7.2 % of the cortex. In contrast, the rSD focus in the TGN+Bum and DCPIB groups was much more confined (Fig. 14E). Taken together, the inhibition of astrocyte swelling by TGN-020 + Bum or DCPIB evidently blocked SiD evolution.

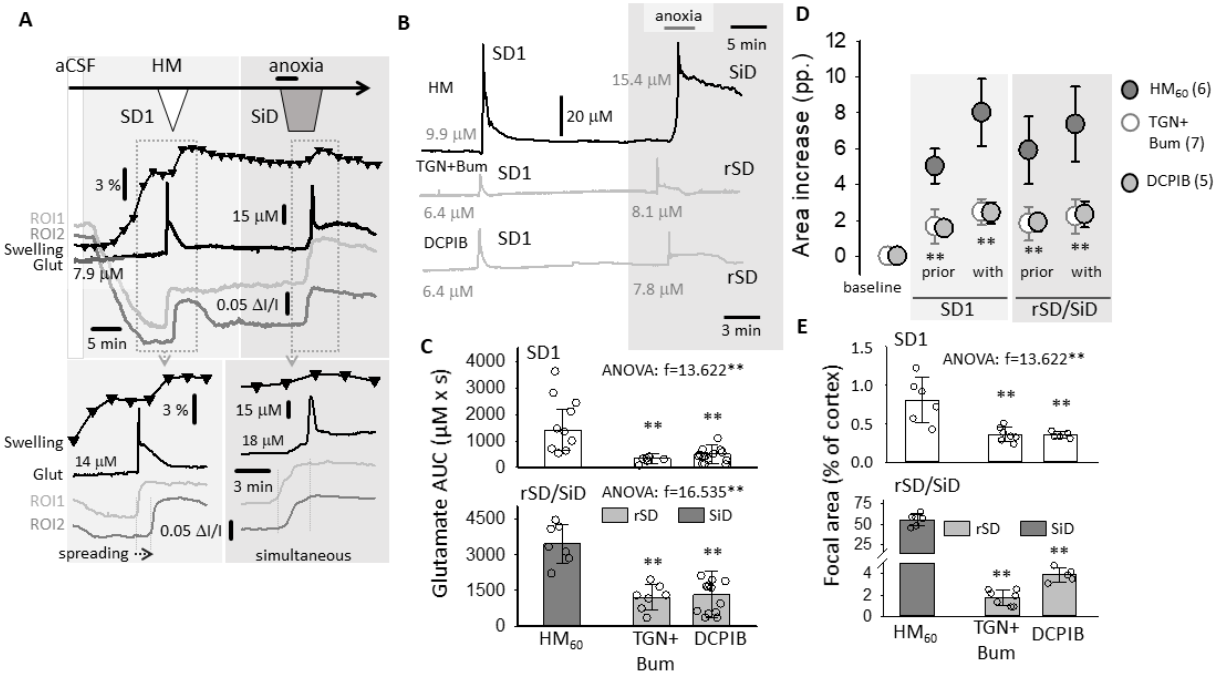

Figure 14. Inhibition of glial swelling or volume regulated glutamate release attenuates SiD. A, Spatiotemporal relationship between tissue swelling (black trace with black triangles), depolarization events (IOS intensity changes at ROI1 and ROI2, gray traces), and changes in glutamate concentration (black trace) in brain slices. **B,** Representative extracellular glutamate concentration traces during SD and SiD in brain slice preparations. **C,** The accumulation of glutamate with SD1 and rSD/SiD (area under the curve, AUC). **D,** The impact of pharmacological treatments on slice swelling relative to baseline at selected time points. **E,** The impact of pharmacological treatments on the size of the focal area of SD1 and rSD/SiD relative to the area of the cortex. Data in C, D, E are given as mean±stdev. Dot plots in C and E shown individual values. Statistical analysis was conducted with a Shapiro-Wilk normality test (C, p=0.110; D, p=0.255; E, p=0.050*), and a repeated measures model (D: F_{time}=196.228**; F_{treat}=29.805**) or one-way ANOVA (C p<0.01**) or a Kruskal-Wallis test (E, p<0.01**) followed by a Sidak or a Dunn's post hoc test (B, D, E: p<0.01** vs. HM_{60}). Abbreviations: aCSF; artificial cerebrospinal fluid, SD1; first spreading depolarization, rSD; recurrent SD, SiD; simultaneous depolarization, HM; hypo-osmotic medium, ROI; region of interest.

Next, we asked whether astrocyte dysfunction is sufficient to produce the SiD phenotype in normal aCSF. Fluorocitrate treatment to arrest astrocyte metabolism replicated slice pathology in HM; (i) the SD elicitation threshold decreased (Fig. 12E); (ii) SD1 emerged spontaneously (4 of 5 slices), and (iii) SiD evolved upon subsequent anoxia (3 of 5 slices) (Fig. 15A). In line with these data, inhibition of astrocyte EAAT2 caused profound extracellular glutamate accumulation to 29.5±9.9 µM, which was followed by a SiD (3 of 4 slices) (Fig. 15B). Extracellular glutamate accumulation with SiD peaked at 65.3±18.1 µM, followed by further extracellular glutamate accumulation without any recovery. These data further substantiated that extracellular glutamate accumulation (due to intensified release or impaired uptake by swollen astroglia) must have mediated SiD in HM.

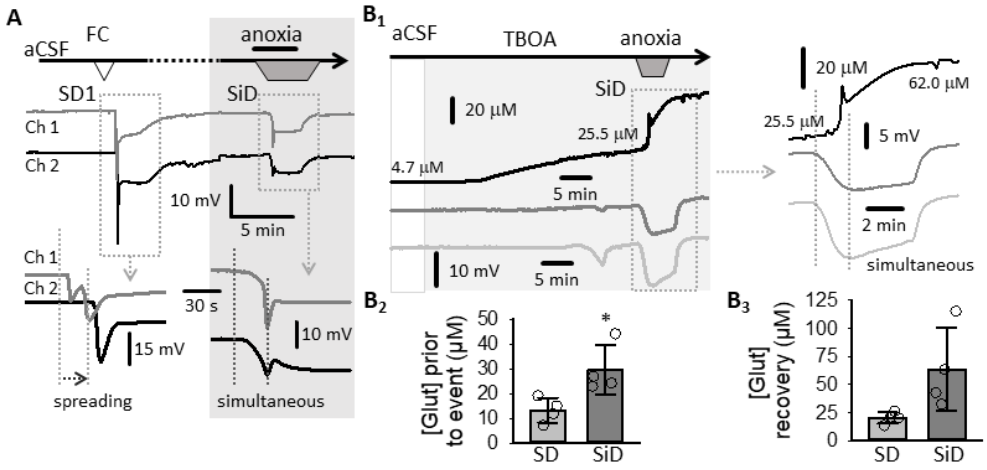

Figure 15. Fluorocitrate treatment reproduced the SiD phenotype; TBOA treatment caused profound extracellular glutamate accumulation and SiD. A, The application of fluorocitrate (FC) to brain slices replicated the SiD phenotype is aCSF. **B,** Representative recordings of glutamate concentration (Glut) and DC potential (Ch1 and Ch2) under TBOA treatment – note the occurrence of SiD (B_1), and high glutamate concentration at two selected phases of these experiments (B_{2-3}). Data in B_{2-3} are given as mean±stdev. Dot plots in B_{2-3} shown individual values. Statistical analysis was conducted with a Shapiro-Wilk normality test (B_2, p=0.158; B_3, p=0.127) and one-way ANOVA (B_{2-3}; p<0.01**) followed by a Sidak post hoc test (B: p<0.05* vs. SD). Abbreviations: aCSF; artificial cerebrospinal fluid, SD1; first spreading depolarization, rSD; recurrent SD, SiD; simultaneous depolarization, HM; hypo-osmotic medium, ROI; region of interest, FC; fluorocitrate.

To determine the source of surplus glutamate accumulated in the extracellular space during tissue swelling AMPA, NMDA and kainate receptors were blocked. The antagonism of ionotropic glutamate receptors was partially effective against SiD, but was ineffective against slice swelling in HM (Fig. 16). Furthermore, glutamate receptor antagonists were the least effective against extracellular glutamate accumulation. Under CNQX+MK-801 incubation, multifocal rSDs occurred, as seen in a few HM slices before (Fig. 11). These observations confirmed the pivotal role of astrocytes in tissue swelling and suggest that surplus glutamate of astrocyte origin, in addition to neuronal release, must be implicated in the evolution of SiD.

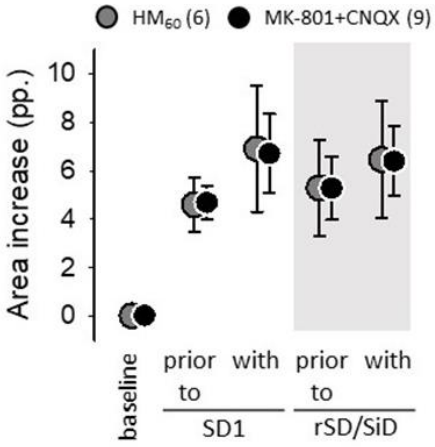

Figure 16. Glutamate receptor antagonism during hypo-osmotic challenge. The antagonisms of ionotropic glutamate receptors by MK-801 and CNQX was ineffective against tissue swelling. Slice area was expressed relative to baseline at selected time points. Data are given as mean±stdev; the number of events analyzed is shown in the legend. Abbreviations: SD1; first spreading depolarization, rSD; recurrent SD, SiD; simultaneous depolarization, HM; hypo-osmotic medium.

3.2.5. Hyperosmotic treatment reverses tissue swelling, restores physiological extracellular glutamate concentration, and prevents SiD

Taken the results above, we hypothesized that the complete reversal of cellular edema by hyperosmotic treatment could restore extracellular glutamate levels to the physiological range, and prevent SiD. To test this hypothesis, HM was substituted with HRM after 30 min HM incubation, and the slice was challenged with anoxia as above.

HRM completely reversed slice swelling, restored physiological extracellular glutamate concentration, and promoted the recovery of the IOS signal (Fig. 17A center).

Further, HRM exposure completely prevented the occurrence of any depolarization and extracellular glutamate accumulation upon anoxia (Fig 17A right). The electrical threshold of SD elicitation was also markedly increased under HRM (2422.5±341.7 vs. 54.0±2.1 vs. 1220.0±6.2 μC, HRM vs. HM_{100} vs. aCSF) (Fig. 17B). The coincidence between slice swelling and extracellular glutamate concentration was further supported by their strong positive linear correlation (r=0.819**) (Fig. 17C). We concluded that extracellular glutamate content was tightly coupled to tissue edema, and that anti-edema treatment effectively counteracted extracellular glutamate accumulation and SiD.

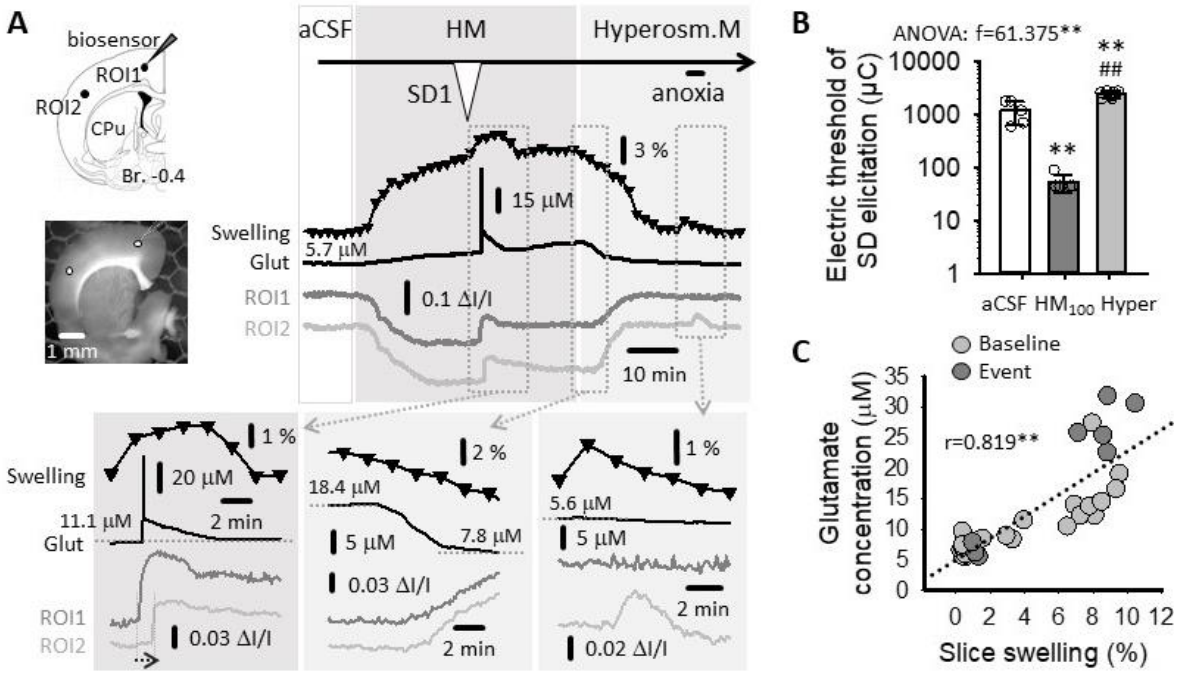

Figure 17. Reversal of slice swelling and SiD to SD with hyperosmotic medium (HRM). A, Changes of extracellular glutamate (Glut) accumulation and the IOS signal (ROI1 & ROI2) after HRM treatment. **B,** The impact of HRM on the electrical threshold of SD elicitation, with respect to aCSF and HM_{100}. **C,** Correlation between glutamate concentration and slice swelling. Data in B are given as mean±stdev. After a Shapiro-Wilk test of normality (p=0.494), statistical analysis relied on a one-way ANOVA and a Sidak post hoc test ($p<0.01$** vs. aCSF, $p<0.01^{\#\#}$ vs. HM_{100}), and a one-tailed Pearson correlation analysis (C). Abbreviations: aCSF; artificial cerebrospinal fluid, SD1; first spreading depolarization, HM; hypo-osmotic medium; ROI; region of interest.

4. Discussion

Acute brain slice preparations yield a reliable and reproducible approach for modelling both physiological and pathological states in the brain. Here we examined the temporal and spatial SD features with electrophysiological and imaging techniques. Moreover, we investigated the cell-damaging effects of SD by histological analysis. Our experiments were the first to evaluate LFP and IOS features of SD under severe metabolic crisis compared to physiological condition. In our experiments we provided large scale (mm) whole slice IOS measurements for an accurate visualization of SD propagation. We demonstrated that SDs in metabolically compromised tissue engaged considerable area of the cortex and caused significant neuronal loss. Furthermore, in our *in vitro* edema model we defined that tissue swelling impairs astrocytic clearance capacity and promotes neuronal hyper-excitability. The impairment of astrocyte function strongly contributes to the simultaneous depolarization of an extended tissue volume and results in extensive cellular loss.

4.1. Comparative analysis of spreading depolarizations under osmotic or metabolic stress

Here we set out to provide a comparative analysis of SD evolution on live brain slices, in response to selected SD triggers and in various media, under otherwise standardized experimental conditions. In this experimental project we aimed to explore the electrophysiological together with the intrinsic optical signal features of SDs under global oxygen-glucose deprivation or osmotic stress with respect to the physiological condition. The histological consequences of SD under these states were also evaluated (Fig. 18)[53].

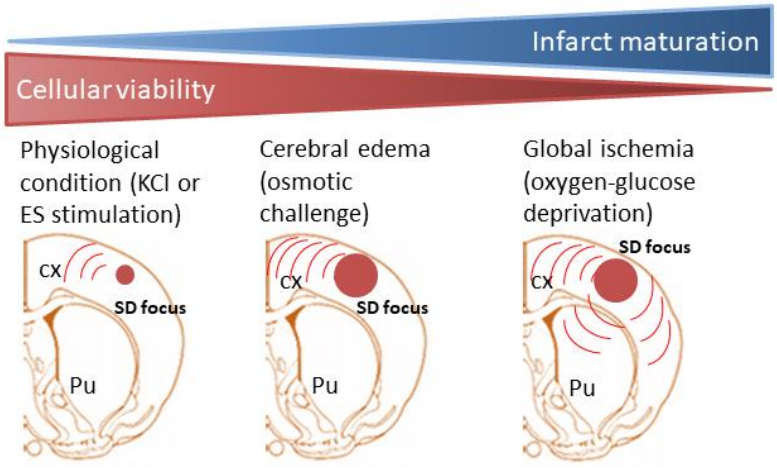

Figure 18. Graphical summary of the applied experimental approaches and the main findings of the study. Schematic drawings depict the propagation (red curves) and focal area (red circles) of SDs among physiological and pathological conditions. SDs elicited by KCl and ES (i.e. physiological condition) have punctual focus and affect restricted area of the cortex. In contrast, SDs induced by hypo-osmotic or ischemic challenge affect enlarged tissue volume and have extended focal area. Note that, cellular viability shows negative correlation while infarct maturation is coherent with the severity of disease state. Abbreviations: ES; bipolar electric field stimulation, KCl; microinjection of 1M KCl solution, cx: cerebral cortex, Pu: putamen.

4.1.1. Relevance of the applied experimental approaches

SDs elicited with the focal application of 1 M KCl or bipolar electric stimulation in slices bathed in aCSF were used as reference. The application of OGD to study SD was justified by its widespread use to mimic severe global ischemia (e.g. cardiac arrest) or conditions prevalent in the ischemic core in focal cerebral ischemia[55, 84]. Of note, the less commonly implemented, partial metabolic challenge of submerged slices may be relevant to recapitulate ischemic penumbra conditions, although this model was reported not to give rise to spontaneous SDs[63]. Further, mild or severe hypoxia at normal glucose levels has long been known to trigger SD, but this condition should not be confused with ischemia (i.e. ischemia is the restricted availability of oxygen, as well as glucose)[85]. To study the impact of osmotic stress on SD, we incubated the brain slices in HM, following a previously established approach to model cerebral edema progression[53, 57, 86]. We experimented with HM solutions of decreasing Na^+ content in our pilot experiments (120-100-80-60-40 mM, HM_{120}-HM_{40}, respectively), and selected here HM_{60} for systematic work, because incubation of the slices in HM_{60} reliably produced SD within 10 min after HM application. Higher Na^+ concentration HM solutions in our pilot experiments (e.g. HM_{100}) also caused SD occurrence, but at more variable and typically longer latency. The used Na^+ concentration may occur spatio-temporally locked with SD in the *in vivo* brain, as the extracellular concentration of Na^+ has been known to decrease from 140-150 mM

down to 50-70 mM with SD[87]. The SD-linked osmotic stress, however, must be less pronounced, due to the compensatory accumulation of osmolites other than Na^+ in the interstitium (e.g. K^+ and glutamate)[14, 87]. Finally, as control for both OGD and HM, we elicited SD in aCSF with highly focused KCl pressure injection (picoliter volume), expected to be near the minimum conditions of SD elicitation, and the least invasive[10]. This condition is thought to be relevant to model SD as it occurs in migraine with aura[88]. In other aCSF-incubated slices, electrical stimulation was applied for SD elicitation, due to its frequent application in a number of labs with the purpose to determine the threshold of SD elicitation[66, 89]. The otherwise standardized conditions (i.e. the level of the coronal brain slices, the region studied, the composition and temperature of the media, the type of the brain slice chamber and the standard approach of data acquisition) allowed the identification of SD features that occur typically in response to these well-defined and reliably reproducible osmotic or ischemic challenges.

4.1.2. SDs under osmotic and metabolic stress invaded extended cortical area and reduced cellular viability

Both OGD and HM gave rise to a spontaneous, long-lasting SD, at a short latency as previously shown (2.7-9.2 min)[63, 90]. These spontaneous events propagated over the entire cortical area in the preparation. The brain slice was irresponsive to further stimulation after SD in OGD, and displayed acute, extensive histological damage in the path of SD (Fig. 8), therefore SD has been accepted as a terminal event in the cortex during OGD. These results agree with earlier findings[90, 91]. In contrast, the tissue repolarized from the SD in HM – albeit with a long delay (Fig. 6) – confirming previous observations[53, 86, 92]. The partial electrophysiological regeneration was supported by the propensity of the tissue to bear subsequent SDs either spontaneously occurring in HM (Fig. 6) or triggered with transient anoxia in HM[53, 86]. In line with the functional data, the first SD in HM caused cellular injury in the cortex engaged in SD, but the damage was less severe than that seen after SD in OGD (Fig. 8). SD evoked by OGD sustained for 15-20 min here was associated with extensive injury in all layers of the cortex as evidenced by TTC staining (Fig. 8A), and in line with previous reports[90, 91]. Yet, some cortical neurons (e.g. in layer 4) may survive shorter OGD (about 10 min) followed by reperfusion with normal aCSF, and not reach the commitment point to neuronal death, as shown by patch clamp recordings[93]. Also, subcortical structures, such as neuron populations in the hypothalamus and the brain stem may be more resistant to OGD than the cortex[91, 94]. In the control conditions here (KCl or ES), a train of 4-5 short-lasting SDs could be elicited at an interval of 10-12 min in agreement with previous reports[62], which demonstrates the sustained viability of the tissue

after the passage of SD under physiological conditions. Of the two control conditions here, focal low volume KCl application with pressure injection caused no detectable histological degeneration in the brain slice. However, ES-triggered SDs were accompanied with obvious damage to the tissue. Although not documented systematically, most SD researchers agree that electric stimulation with a charge sufficient to trigger SD leaves focal necrotic tissue damage behind at the electrode contact point[95]. This is also substantiated by the need to reposition the stimulating electrode between SDs evoked to estimate the electric SD threshold reliably[66].

4.1.3. SDs elicited by various stimuli represent different stages of the SD continuum

Collectively, our results here present three stages of the SD continuum[95]: (i) apparently harmless SD in intact tissue followed by sufficient repolarization and recovery, (ii) injurious SD with poor repolarization and recovery emerging under osmotic stress, and (iii) terminal and detrimental SD with no repolarization in oxygen and glucose deprived tissue. The distinct features of the negative DC shift and IOS signature of SD may disclose some mechanistic elements of SD evolution typical for the homeostatic conditions. For example, the slower rate of repolarization in HM and OGD as seen here (Fig. 6) is thought to correspond to the dysfunctional re-uptake of K^+ or glutamate. The shortage of ATP in OGD causes the failure of the neuronal and astrocytic Na^+/K^+ ATP-ase, which hampers the uptake of K^+ accumulated with the SD wave front in the extracellular space[3, 96]. Although osmotic stress could also attenuate the enzymatic activity of the Na^+/K^+ ATP-ase[97], HM exposure has been shown to induce prominent astrocyte swelling[53, 81, 86] and to disrupt the astrocyte buffer capacity, reflected by a progressive accumulation of glutamate, for example[53, 86]. Astrocytic K^+ and glutamate re-uptake has been implicated in the repolarization after SD[98]. Taken together, we propose that the plausible cause of slower repolarization and prolonged SD duration in HM was the injured glial K^+ clearance and glutamate transport. The failure of the Na^+/K^+ ATP-ase and the exhaustion of the astroglial buffer capacity are also suspected to contribute to the remarkably greater area engaged in SD propagation in HM and OGD compared to aCSF (Fig. 7). SD in HM stood out from the other experimental conditions with its high rate of propagation and DC shift amplitude (Fig. 6-7).

Since SDs induced by osmotic stress represent a transition between SDs in normal tissue and terminal SDs elicited by OGD in our following experiments we set out to explore the underlying mechanisms of hypo-osmotic SDs.

4.2. Observation of simultaneous depolarization in brain slices

Next, we applied hypo-osmotic treatment together with anoxia to create ischemic swelling in brain slices. We performed extensive pharmacological manipulations and electrophysiological recordings together with extracellular glutamate measurements and histological analysis to understand the mechanistic background of SD in acute tissue swelling.

Here we present novel observations in brain slices that the simultaneously depolarized tissue volume denoting the focus of an SD event (i.e. simultaneous depolarization, SiD) may become extensive (>2 mm^2) rather than punctual (<1 mm^2) during acute ischemic tissue swelling. We demonstrate that malignant astrocyte swelling promotes SiD evolution and neuron death in our edema model. We further show that SiD encompasses tissue that has previously participated in the propagation of an SD, causing the subsequent aggravation of histological damage. However, the mitigation of astrocyte swelling by pharmacological treatment or by hyper-osmotic therapy prevented SiD. Taken together, our data demonstrate the intensified pathogenic potential of SD during acute edema formation (Fig. 19).

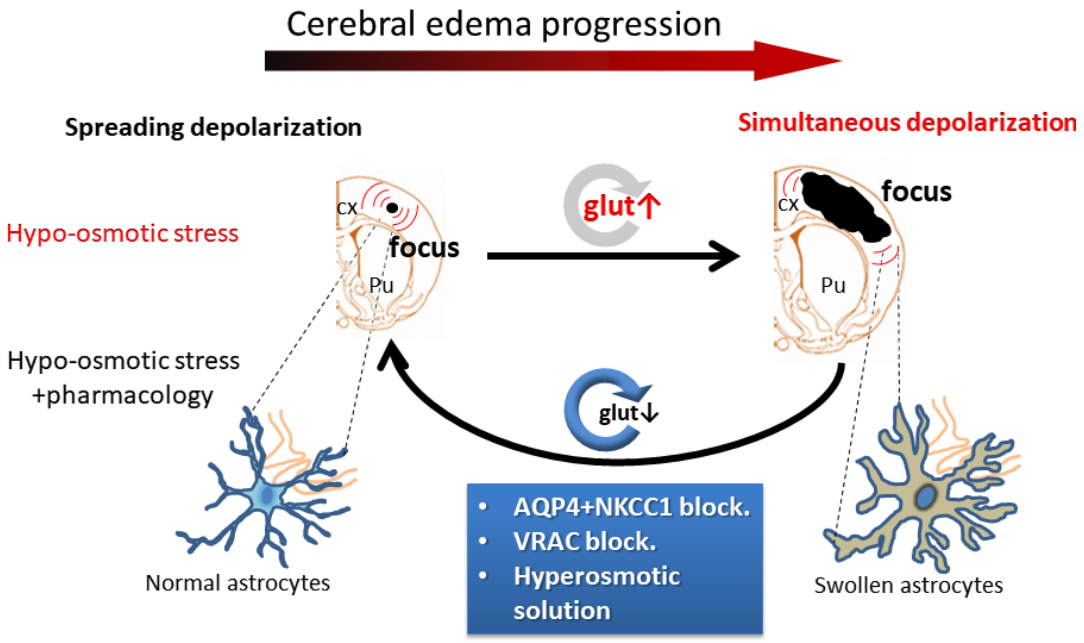

Figure 19. Attenuation of acute brain swelling hampers the evolution of simultaneous depolarization. Schematic drawings illustrate cerebral edema progression in brain slices exposed to hypo-osmotic stress. In the acutely swollen brain SiD represents an extended SD focus due to the impaired glutamate clearance of swollen astrocytes. Attenuation of (i) glial swelling by AQP4 +NKCC blockade, (ii) volume regulated glutamate release by VRAC antagonism or (iii) application of hyper-osmotic mannitol prevent the evolution SiD. Abbreviations: cx; cerebral cortex, Pu; putamen, AQP4: aquaporin-4 channel, NKCC1: $Na^+/K^+/Cl^-$ co-transporter 1, VRAC: volume regulated anion channel.

4.2.1. SiD is the pathological expansion of prior SD foci in brain slices exposed to osmotic stress

Cerebral edema produced experimentally is a sufficient condition for SD to occur spontaneously, which predisposes the tissue covered by the propagating SD for an upcoming SiD. The tissue volume engaged in the SiD then serves as an extensive focus of an SD event taking off from its perimeter. In particular, SiD is predicted by the swelling of astrocytes in edematous tissue. Astrocyte swelling under hypo-osmotic stress is implicated in the excessive extracellular accumulation of glutamate, coincident with SiD occurrence. Further, SiD is followed by the oncotic cell death of neurons and astrocytes, suggestive of injury maturation associated with SiD. Finally, hyperosmotic intervention reduces the susceptibility of the nervous tissue to SD, and fully prevents the cascade of events leading to SiD.

These are the first experiments to characterize SiD comprehensively. An early review by Marshall (1959) did raise the possibility of SiD encompassing the entire cortex, but without providing any supportive experimental evidence[99]. SiD-like events were later recorded in brain slice preparations incubated in hypo-osmotic medium and challenged with hypoxia or in response to the bath application of supra-physiological concentration NMDA, but without detailed analysis of the phenomenon or realizing its significance[90, 100]. It is of high importance that an SiD-like event has been recently captured in the severely injured human brain[101]. In the ischemic penumbra of a malignant hemispheric stroke, terminal depolarization in the wake of circulatory arrest was seen to arrive with an unusual short delay from electrode to electrode on the subdural strip, when the strip was positioned at an already compromised area of the cortex. This observation suggests that SiD is clinically relevant, and gives ample momentum to study the pathophysiological relevance of SiD in more detail. Future clinical studies may attempt to associate particular patterns of SD occurrence with brain edema formation.

4.2.2. Astrocyte swelling plays a key role in the evolution of SiD

Brain slices were exposed to severe osmotic stress achieved by the lowering of $[Na^+]$ of the incubation medium to 100 or 60 mM[65]. SiD in our study occurred invariably superimposed on tissue edema, a condition to affect astrocytes first. The attention to astrocytes was also substantiated by our finding that fluorocitrate treatment caused astrocyte swelling and reproduced SiD evolution. Astrocytes are more permeable to water than neurons because astrocytes are endowed with AQP4 water channels at their processes, which conduct osmotically driven water[102, 103]. Further, astrocytes have been found to swell in response to ischemia or SD, which is thought to represent water movement via AQP4 along inward K^+

currents[33, 104]. Alternatively, neurons and astrocytes are both affected by the SD-related cytotoxic swelling due to excess chloride entry through NKCC[81, 104, 105]. We found that HM-exposed astrocytes were markedly swollen in histological preparations, and that the blockade of AQP4 channels and NKCCs prevented tissue edema and SiD occurrence under hypo-osmotic stress. These data collectively demonstrate that astrocyte swelling must be central to SiD evolution. Astrocytic swelling has been implicated in volume regulated glutamate release through glutamate-permeable VRACs[40, 83, 106]. At the same time, the significant glutamate uptake through astrocytic Na^+- and ATP-dependent EAAT2 is impaired under metabolic stress, which sustains high extracellular glutamate concentration[50, 107, 108]. The inhibition of VRACs in our experiments prevented the extracellular accumulation of glutamate, reduced the focal area of depolarization and the likelihood of SiD occurrence. Conversely, EAAT2 blockade alone reproduced the SiD phenotype as seen under HM incubation. The antagonism of AMPA and NMDA receptors was partially effective against SiD, and resulted in multifocal SD evolution. These results suggest that surplus extracellular glutamate of astrocyte origin, in addition to neuronal release, must be implicated in the evolution of SiD. This seems plausible taken that glutamate appears to contribute to SD propagation, although several arguments cast doubt on the role of glutamate as the mediator driving the propagation of the SD wavefront[14, 109, 110]. Previous observations suggest that even with only a very low residual blood flow, SD must last longer than 10 min before cell death occurs[111]. Our histological results suggest that this time span is significantly shortened when astrocytic function is already disturbed before the onset of neuronal depolarization. Thus, although SD is a primarily neuronal phenomenon, our findings substantiate the outstanding importance of astrocytes as protective guarantors against the devastating effects of SD[95, 112-114].

The clinical management of cerebral edema in acute brain injury currently aims at the reduction of intracranial pressure and the maintenance of cerebral perfusion pressure by sedation, hyperventilation, osmotherapy, hypothermia, and in the most severe cases decompressive craniectomy[115-117]. However, for example, in severe subarachnoid hemorrhage intravenous high sodium fluids are administered increasingly more frequently because hypo-osmolarity is suggested to increase the risk and severity of delayed ischemic injury[118].

5. Main observations and conclusions

- We show here that under otherwise standardized experimental conditions, SD is most pronounced in HM, in which condition the metabolic substrate supply is unlimited, but the tissue is hyper excitable due to cellular swelling and impaired glutamate clearance. In contrast with OGD, SD propagating under hypo-osmotic condition is not terminal, yet it is associated with irreversible tissue injury. Our results yield a new perspective by the direct comparison of these two states, which must co-exist and intertwine in acute brain injury.
- We confirm in rat brain slices exposed to osmotic stress that SiD is the pathological expansion of prior punctual SD foci (0.5-1 mm^2), is associated with astrocyte swelling, and triggers cell death. The blockade of astrocytic AQP4 and NKCCs or VRACs mitigated slice edema, extracellular glutamate accumulation (<10 μM) and SiD occurrence. In contrast, inhibition of glial metabolism or inhibition of astrocyte glutamate transporters reproduced the SiD phenotype.

Finally, *in vitro* models, as presented here, offer an opportunity to screen the neuroprotective potential of therapeutically promising drug candidates, before testing them in *in vivo* systems. The pharmacological modulation of neurophysiological events that take place in the first minutes after acute brain injury may not seem clinically relevant. Yet, it must be realized that with the maturation of the injury, SDs become recurrent and at least some of them originating at the peri-infarct zone share basic features with the initial SD[13]. Our results that preventive hyperosmotic intervention reduced the excitability of the nervous tissue and most importantly, averted SiD, provide pathophysiological insight into this empirical clinical strategy for the first time, and emphasize the need to invent new ways of preventive osmotherapy in the treatment of acute brain injury.

Therefore, experimentation in these simple model systems is expected to impart valuable understanding of SD pathophysiology, effectively complement *in vivo* work, and identify potential sites for intervention.

6. Summary

Background: Recurrent spreading depolarizations (SDs) occur in stroke and traumatic brain injury and are considered as hallmarks of injury progression. SDs are also associated with cerebral edema which leads to worse clinical outcome. Due to the complexity of conditions associated with SD in the living brain we set out to provide a comparative evaluation of SD evolution in brain slices, in response to selected SD triggers and in various media. Next, we aimed to create acute edematous-ischemic condition in brain slices and to assess the role of astrocytes in the evolution of simultaneous depolarization and neuronal excitability.

Methods: Coronal brain slices (350 μm) prepared from Wistar and Sprague-Dawley rats (n=98) were used for the experiments. Hypo-osmotic medium (Na^+ content reduced from 130 to 60 mM, HM) or oxygen-glucose deprivation (OGD) were applied to create edema or ischemic challenge. Brain slices superfused with artificial cerebrospinal fluid (aCSF) served as control condition. SDs were evoked in the control group with pressure injection of KCl or electric stimulation. Bumetanide (1 mM), TGN-020 (100 μM) and DCPIB (20 μM) were administered to block NKCCs, AQP4 and VRACs. NMDA+AMPA/kainate receptor receptors were blocked by MK-801 (100 μM)+CNQX (20 μM), EAAT2 were inhibited by TFB-TBOA (10 μM and 100 μM). Fluorocitrate (0.5- 1 mM) was used to paralyze astrocyte metabolism by the disruption of citrate cycle. LFP was recorded via glass capillary electrode, IOS imaging was conducted at white light illumination to characterize temporal and spatial features of SD. Extracellular glutamate concentration was measured with glutamate biosensor. Electron microscopy, TTC, Golgi-Cox and hematoxylin-eosin staining were used to assess tissue damage.

Results: Severe osmotic stress or OGD provoked a spontaneous SD. In contrast with SDs triggered in aCSF, these spontaneous depolarizations were characterized by incomplete repolarization and prolonged duration. Further, SDs under HM or OGD propagated over the entire cortex and occasionally invaded the striatum, while SDs in aCSF covered a significantly smaller cortical area before coming to a halt, and never spread to the striatum. SDs in HM displayed the greatest amplitude and the most rapid propagation velocity. Spontaneous SD in HM and especially under OGD was followed by intense tissue injury. We also observed that after a spontaneous SD in HM an extended cortical area depolarized simultaneously upon anoxia. SiD evolved from an enlarged focus, which was engaged by a previous SD and caused

prominent swelling of astrocytes. SiD was associated with cytotoxic glutamate accumulation, triggered neuronal hyper-excitability and induced profound cellular loss. The pharmacological blockade of astrocyte swelling by TGN-020+Bum or by DCPIB reduced slice edema, extracellular glutamate accumulation and prevented SiD occurrence. However, the blockade of ionotropic glutamate receptors was ineffective against SiD. Also, hyperosmotic mannitol counteracted extracellular glutamate accumulation and prevented SiD. In contrast, inhibition of glial metabolism or inhibition of astrocyte glutamate transporters reproduced the SiD phenotype.

Conclusions: Our results demonstrate that the exhaustion of astrocyte buffering capacity and the related neuronal hyper-excitability are responsible for the mass depolarization of the cerebral cortex. These data conclude the neurotoxic role of swollen astrocytes and propose the pharmacological attenuation of glial swelling to preserve normal neuronal signaling. Finally, our results highlight the importance of acute hyper-osmotic treatment as a potential neuroprotective therapy in cerebrovascular disease states.

7. References

1. Grysiewicz RA, Thomas K, Pandey DK. Epidemiology of ischemic and hemorrhagic stroke: incidence, prevalence, mortality, and risk factors. Neurol Clin. 2008;26(4):871-95, vii.
2. Hartings JA, Rolli ML, Lu XC, Tortella FC. Delayed secondary phase of peri-infarct depolarizations after focal cerebral ischemia: relation to infarct growth and neuroprotection. The Journal of neuroscience : the official journal of the Society for Neuroscience. 2003;23(37):11602-10.
3. Dreier JP. The role of spreading depression, spreading depolarization and spreading ischemia in neurological disease. Nature medicine. 2011;17(4):439-47.
4. Somjen GG. Mechanisms of spreading depression and hypoxic spreading depression-like depolarization. Physiological reviews. 2001;81(3):1065-96.
5. Leao A. Spreading depression of activity in the cerebral cortex. J Neurophysiol. 1944;7: 359–390.
6. Leao AA. Further observations on the spreading depression of activity in the cerebral cortex. Journal of neurophysiology. 1947;10(6):409-14.
7. Dijkhuizen RM, Beekwilder JP, van der Worp HB, Berkelbach van der Sprenkel JW, Tulleken KA, Nicolay K. Correlation between tissue depolarizations and damage in focal ischemic rat brain. Brain research. 1999;840(1-2):194-205.
8. Matsuura T, Bures J. The minimum volume of depolarized neural tissue required for triggering cortical spreading depression in rat. Experimental brain research. 1971;12(3):238-49.
9. Verhaegen MJ, Todd MM, Warner DS, James B, Weeks JB. The role of electrode size on the incidence of spreading depression and on cortical cerebral blood flow as measured by H2 clearance. Journal of cerebral blood flow and metabolism : official journal of the International Society of Cerebral Blood Flow and Metabolism. 1992;12(2):230-7.
10. Tang YT, Mendez JM, Theriot JJ, Sawant PM, Lopez-Valdes HE, Ju YS, et al. Minimum conditions for the induction of cortical spreading depression in brain slices. Journal of neurophysiology. 2014;112(10):2572-9.
11. Koroleva VI, Bures J. Circulation of cortical spreading depression around electrically stimulated areas and epileptic foci in the neocortex of rats. Brain research. 1979;173(2):209-15.
12. Mies G. Blood flow dependent duration of cortical depolarizations in the periphery of focal ischemia of rat brain. Neuroscience letters. 1997;221(2-3):165-8.
13. Hartings JA, Shuttleworth CW, Kirov SA, Ayata C, Hinzman JM, Foreman B, et al. The continuum of spreading depolarizations in acute cortical lesion development: Examining Leao's legacy. Journal of cerebral blood flow and metabolism : official journal of the International Society of Cerebral Blood Flow and Metabolism. 2017;37(5):1571-94.
14. Pietrobon D, Moskowitz MA. Chaos and commotion in the wake of cortical spreading depression and spreading depolarizations. Nature reviews Neuroscience. 2014;15(6):379-93.
15. Hartings JA, Bullock MR, Okonkwo DO, Murray LS, Murray GD, Fabricius M, et al. Spreading depolarisations and outcome after traumatic brain injury: a prospective observational study. The Lancet Neurology. 2011;10(12):1058-64.
16. Dreier JP, Woitzik J, Fabricius M, Bhatia R, Major S, Drenckhahn C, et al. Delayed ischaemic neurological deficits after subarachnoid haemorrhage are associated with clusters of spreading depolarizations. Brain : a journal of neurology. 2006;129(Pt 12):3224-37.
17. Lauritzen M, Dreier JP, Fabricius M, Hartings JA, Graf R, Strong AJ. Clinical relevance of cortical spreading depression in neurological disorders: migraine, malignant stroke, subarachnoid and intracranial hemorrhage, and traumatic brain injury. Journal of cerebral blood

flow and metabolism : official journal of the International Society of Cerebral Blood Flow and Metabolism. 2011;31(1):17-35.
18. Dreier JP, Fabricius M, Ayata C, Sakowitz OW, Shuttleworth CW, Dohmen C, et al. Recording, analysis, and interpretation of spreading depolarizations in neurointensive care: Review and recommendations of the COSBID research group. Journal of cerebral blood flow and metabolism : official journal of the International Society of Cerebral Blood Flow and Metabolism. 2017;37(5):1595-625.
19. Klass A, Sanchez-Porras R, Santos E. Systematic review of the pharmacological agents that have been tested against spreading depolarizations. Journal of cerebral blood flow and metabolism : official journal of the International Society of Cerebral Blood Flow and Metabolism. 2018;38(7):1149-79.
20. Karatas H, Erdener SE, Gursoy-Ozdemir Y, Lule S, Eren-Kocak E, Sen ZD, et al. Spreading depression triggers headache by activating neuronal Panx1 channels. Science. 2013;339(6123):1092-5.
21. Harriott AM, Chung DY, Uner A, Bozdayi RO, Morais A, Takizawa T, et al. Optogenetic Spreading Depression Elicits Trigeminal Pain and Anxiety Behavior. Annals of neurology. 2021;89(1):99-110.
22. Nedergaard M, Hansen AJ. Spreading depression is not associated with neuronal injury in the normal brain. Brain research. 1988;449(1-2):395-8.
23. Klatzo I. Brain oedema following brain ischaemia and the influence of therapy. Br J Anaesth. 1985;57(1):18-22.
24. Leinonen V, Vanninen R, Rauramaa T. Cerebrospinal fluid circulation and hydrocephalus. Handb Clin Neurol. 2017;145:39-50.
25. Unterberg AW, Stover J, Kress B, Kiening KL. Edema and brain trauma. Neuroscience. 2004;129(4):1021-9.
26. Risher WC, Andrew RD, Kirov SA. Real-time passive volume responses of astrocytes to acute osmotic and ischemic stress in cortical slices and in vivo revealed by two-photon microscopy. Glia. 2009;57(2):207-21.
27. Badaut J, Nehlig A, Verbavatz J, Stoeckel M, Freund-Mercier MJ, Lasbennes F. Hypervascularization in the magnocellular nuclei of the rat hypothalamus: relationship with the distribution of aquaporin-4 and markers of energy metabolism. J Neuroendocrinol. 2000;12(10):960-9.
28. Simard JM, Kent TA, Chen M, Tarasov KV, Gerzanich V. Brain oedema in focal ischaemia: molecular pathophysiology and theoretical implications. The Lancet Neurology. 2007;6(3):258-68.
29. O'Donnell ME, Tran L, Lam TI, Liu XB, Anderson SE. Bumetanide inhibition of the blood-brain barrier Na-K-Cl cotransporter reduces edema formation in the rat middle cerebral artery occlusion model of stroke. Journal of cerebral blood flow and metabolism : official journal of the International Society of Cerebral Blood Flow and Metabolism. 2004;24(9):1046-56.
30. Ribeiro Mde C, Hirt L, Bogousslavsky J, Regli L, Badaut J. Time course of aquaporin expression after transient focal cerebral ischemia in mice. J Neurosci Res. 2006;83(7):1231-40.
31. Clement T, Rodriguez-Grande B, Badaut J. Aquaporins in brain edema. J Neurosci Res. 2020;98(1):9-18.
32. Badaut J, Verbavatz JM, Freund-Mercier MJ, Lasbennes F. Presence of aquaporin-4 and muscarinic receptors in astrocytes and ependymal cells in rat brain: a clue to a common function? Neuroscience letters. 2000;292(2):75-8.
33. Risher WC, Croom D, Kirov SA. Persistent astroglial swelling accompanies rapid reversible dendritic injury during stroke-induced spreading depolarizations. Glia. 2012;60(11):1709-20.

34. Sofroniew MV, Vinters HV. Astrocytes: biology and pathology. Acta Neuropathol. 2010;119(1):7-35.
35. Amedee T, Robert A, Coles JA. Potassium homeostasis and glial energy metabolism. Glia. 1997;21(1):46-55.
36. Somjen GG. Ion regulation in the brain: implications for pathophysiology. Neuroscientist. 2002;8(3):254-67.
37. Kofuji P, Newman EA. Potassium buffering in the central nervous system. Neuroscience. 2004;129(4):1045-56.
38. Leis JA, Bekar LK, Walz W. Potassium homeostasis in the ischemic brain. Glia. 2005;50(4):407-16.
39. Yan Y, Dempsey RJ, Sun D. Expression of Na(+)-K(+)-Cl(-) cotransporter in rat brain during development and its localization in mature astrocytes. Brain research. 2001;911(1):43-55.
40. Jayakumar AR, Norenberg MD. The Na-K-Cl Co-transporter in astrocyte swelling. Metabolic brain disease. 2010;25(1):31-8.
41. Su G, Kintner DB, Sun D. Contribution of Na(+)-K(+)-Cl(-) cotransporter to high-[K(+)](o)- induced swelling and EAA release in astrocytes. Am J Physiol Cell Physiol. 2002;282(5):C1136-46.
42. Lu KT, Cheng NC, Wu CY, Yang YL. NKCC1-mediated traumatic brain injury-induced brain edema and neuron death via Raf/MEK/MAPK cascade. Crit Care Med. 2008;36(3):917-22.
43. Curtis DR, Johnston GA. Amino acid transmitters in the mammalian central nervous system. Ergeb Physiol. 1974;69(0):97-188.
44. Fonnum F. Glutamate: a neurotransmitter in mammalian brain. Journal of neurochemistry. 1984;42(1):1-11.
45. Bergles DE, Jahr CE. Glial contribution to glutamate uptake at Schaffer collateral-commissural synapses in the hippocampus. The Journal of neuroscience : the official journal of the Society for Neuroscience. 1998;18(19):7709-16.
46. Grant GB, Dowling JE. A glutamate-activated chloride current in cone-driven ON bipolar cells of the white perch retina. The Journal of neuroscience : the official journal of the Society for Neuroscience. 1995;15(5 Pt 2):3852-62.
47. Otis TS, Kavanaugh MP, Jahr CE. Postsynaptic glutamate transport at the climbing fiber-Purkinje cell synapse. Science. 1997;277(5331):1515-8.
48. Kojima S, Nakamura T, Nidaira T, Nakamura K, Ooashi N, Ito E, et al. Optical detection of synaptically induced glutamate transport in hippocampal slices. The Journal of neuroscience : the official journal of the Society for Neuroscience. 1999;19(7):2580-8.
49. Sibson NR, Dhankhar A, Mason GF, Rothman DL, Behar KL, Shulman RG. Stoichiometric coupling of brain glucose metabolism and glutamatergic neuronal activity. Proc Natl Acad Sci U S A. 1998;95(1):316-21.
50. Rossi DJ, Oshima T, Attwell D. Glutamate release in severe brain ischaemia is mainly by reversed uptake. Nature. 2000;403(6767):316-21.
51. Kimelberg HK, Kettenmann H. Swelling-induced changes in electrophysiological properties of cultured astrocytes and oligodendrocytes. I. Effects on membrane potentials, input impedance and cell-cell coupling. Brain research. 1990;529(1-2):255-61.
52. Seki Y, Feustel PJ, Keller RW, Jr., Tranmer BI, Kimelberg HK. Inhibition of ischemia-induced glutamate release in rat striatum by dihydrokinate and an anion channel blocker. Stroke. 1999;30(2):433-40.
53. Menyhart A, Frank R, Farkas AE, Sule Z, Varga VE, Nyul-Toth A, et al. Malignant astrocyte swelling and impaired glutamate clearance drive the expansion of injurious spreading

depolarization foci. Journal of cerebral blood flow and metabolism : official journal of the International Society of Cerebral Blood Flow and Metabolism. 2021:271678X211040056.
54. Mc IH, Buchel L, Cheshire JD. The inorganic phosphate and phosphocreatine of Brain especially during metabolism in vitro. Biochem J. 1951;48(1):12-20.
55. Joshi I, Andrew RD. Imaging anoxic depolarization during ischemia-like conditions in the mouse hemi-brain slice. Journal of neurophysiology. 2001;85(1):414-24.
56. Tong CK, Chesler M. Modulation of spreading depression by changes in extracellular pH. Journal of neurophysiology. 2000;84(5):2449-57.
57. Chebabo SR, Hester MA, Jing J, Aitken PG, Somjen GG. Interstitial space, electrical resistance and ion concentrations during hypotonia of rat hippocampal slices. The Journal of physiology. 1995;487 (Pt 3):685-97.
58. Czeh G, Aitken PG, Somjen GG. Membrane currents in CA1 pyramidal cells during spreading depression (SD) and SD-like hypoxic depolarization. Brain research. 1993;632(1-2):195-208.
59. Dietz RM, Kiedrowski L, Shuttleworth CW. Contribution of Na(+)/Ca(2+) exchange to excessive Ca(2+) loading in dendrites and somata of CA1 neurons in acute slice. Hippocampus. 2007;17(11):1049-59.
60. Wu DC, Chen RY, Cheng TC, Chiang YC, Shen ML, Hsu LL, et al. Spreading Depression Promotes Astrocytic Calcium Oscillations and Enhances Gliotransmission to Hippocampal Neurons. Cerebral cortex. 2018;28(9):3204-16.
61. Menyhart A, Farkas AE, Varga DP, Frank R, Toth R, Balint AR, et al. Large-conductance Ca(2+)-activated potassium channels are potently involved in the inverse neurovascular response to spreading depolarization. Neurobiology of disease. 2018;119:41-52.
62. Anderson TR, Andrew RD. Spreading depression: imaging and blockade in the rat neocortical brain slice. Journal of neurophysiology. 2002;88(5):2713-25.
63. Reinhart KM, Shuttleworth CW. Ketamine reduces deleterious consequences of spreading depolarizations. Experimental neurology. 2018;305:121-8.
64. Percie du Sert N, Hurst V, Ahluwalia A, Alam S, Avey MT, Baker M, et al. The ARRIVE guidelines 2.0: updated guidelines for reporting animal research. The Journal of physiology. 2020;598(18):3793-801.
65. Frank R, Bari F, Menyhart A, Farkas E. Comparative analysis of spreading depolarizations in brain slices exposed to osmotic or metabolic stress. BMC neuroscience. 2021;22(1):33.
66. Hertelendy P, Menyhart A, Makra P, Sule Z, Kiss T, Toth G, et al. Advancing age and ischemia elevate the electric threshold to elicit spreading depolarization in the cerebral cortex of young adult rats. Journal of cerebral blood flow and metabolism : official journal of the International Society of Cerebral Blood Flow and Metabolism. 2017;37(5):1763-75.
67. Igarashi H, Huber VJ, Tsujita M, Nakada T. Pretreatment with a novel aquaporin 4 inhibitor, TGN-020, significantly reduces ischemic cerebral edema. Neurological sciences : official journal of the Italian Neurological Society and of the Italian Society of Clinical Neurophysiology. 2011;32(1):113-6.
68. Kimelberg HK. Astrocytic swelling in cerebral ischemia as a possible cause of injury and target for therapy. Glia. 2005;50(4):389-97.
69. Bourke RS, Waldman JB, Kimelberg HK, Barron KD, San Filippo BD, Popp AJ, et al. Adenosine-stimulated astroglial swelling in cat cerebral cortex in vivo with total inhibition by a non-diuretic acylaryloxyacid derivative. Journal of neurosurgery. 1981;55(3):364-70.
70. Swanson RA, Graham SH. Fluorocitrate and fluoroacetate effects on astrocyte metabolism in vitro. Brain research. 1994;664(1-2):94-100.
71. Spong KE, Chin B, Witiuk KL, Robertson RM. Cell swelling increases the severity of spreading depression in Locusta migratoria. Journal of neurophysiology. 2015;114(6):3111-20.

72. Vasylieva N, Maucler C, Meiller A, Viscogliosi H, Lieutaud T, Barbier D, et al. Immobilization method to preserve enzyme specificity in biosensors: consequences for brain glutamate detection. Analytical chemistry. 2013;85(4):2507-15.
73. Gull S, Ingrisch I, Tausch S, Witte OW, Schmidt S. Consistent and reproducible staining of glia by a modified Golgi-Cox method. Journal of neuroscience methods. 2015;256:141-50.
74. Richter F, Ebersberger A, Schaible HG. Blockade of voltage-gated calcium channels in rat inhibits repetitive cortical spreading depression. Neuroscience letters. 2002;334(2):123-6.
75. Szabo I, O MT, Torok Z, Varga DP, Menyhart A, Frank R, et al. The impact of dihydropyridine derivatives on the cerebral blood flow response to somatosensory stimulation and spreading depolarization. British journal of pharmacology. 2019;176(9):1222-34.
76. O MT, Menyhart A, Frank R, Hantosi D, Farkas E, Bari F. Tissue Acidosis Associated with Ischemic Stroke to Guide Neuroprotective Drug Delivery. Biology. 2020;9(12).
77. Goldlust EJ, Paczynski RP, He YY, Hsu CY, Goldberg MP. Automated measurement of infarct size with scanned images of triphenyltetrazolium chloride-stained rat brains. Stroke. 1996;27(9):1657-62.
78. Bederson JB, Pitts LH, Germano SM, Nishimura MC, Davis RL, Bartkowski HM. Evaluation of 2,3,5-triphenyltetrazolium chloride as a stain for detection and quantification of experimental cerebral infarction in rats. Stroke. 1986;17(6):1304-8.
79. Hatfield RH, Mendelow AD, Perry RH, Alvarez LM, Modha P. Triphenyltetrazolium chloride (TTC) as a marker for ischaemic changes in rat brain following permanent middle cerebral artery occlusion. Neuropathology and applied neurobiology. 1991;17(1):61-7.
80. Chebabo SR, Hester MA, Aitken PG, Somjen GG. Hypotonic exposure enhances synaptic transmission and triggers spreading depression in rat hippocampal tissue slices. Brain research. 1995;695(2):203-16.
81. Kimelberg HK, Rutledge E, Goderie S, Charniga C. Astrocytic swelling due to hypotonic or high K+ medium causes inhibition of glutamate and aspartate uptake and increases their release. Journal of cerebral blood flow and metabolism : official journal of the International Society of Cerebral Blood Flow and Metabolism. 1995;15(3):409-16.
82. Basarsky TA, Feighan D, MacVicar BA. Glutamate release through volume-activated channels during spreading depression. The Journal of neuroscience : the official journal of the Society for Neuroscience. 1999;19(15):6439-45.
83. Yang J, Vitery MDC, Chen J, Osei-Owusu J, Chu J, Qiu Z. Glutamate-Releasing SWELL1 Channel in Astrocytes Modulates Synaptic Transmission and Promotes Brain Damage in Stroke. Neuron. 2019;102(4):813-27 e6.
84. Juzekaeva E, Nasretdinov A, Gainutdinov A, Sintsov M, Mukhtarov M, Khazipov R. Preferential Initiation and Spread of Anoxic Depolarization in Layer 4 of Rat Barrel Cortex. Frontiers in cellular neuroscience. 2017;11:390.
85. Balestrino M, Somjen GG. Chlorpromazine protects brain tissue in hypoxia by delaying spreading depression-mediated calcium influx. Brain research. 1986;385(2):219-26.
86. Ákos Menyhárt RF, Attila E. Farkas, Zoltán Süle, Viktória É. Varga, Ádám Nyúl-Tóth, Anne Meiller, Orsolya Iványkovits-Kiss, Coline L. Lemale, Írisz Szabó, Réka Tóth, Dániel Zölei-Szénási, Johannes Woitzik, Stephane Marinesco, István A. Krizbai, Ferenc Bari, Jens P. Dreier, Eszter Farkas. Malignant astrocyte swelling and impaired glutamate clearance drive the expansion of injurious spreading depolarization foci. 2020.
87. Hansen AJ, Zeuthen T. Extracellular ion concentrations during spreading depression and ischemia in the rat brain cortex. Acta physiologica Scandinavica. 1981;113(4):437-45.
88. Harriott AM, Takizawa T, Chung DY, Chen SP. Spreading depression as a preclinical model of migraine. The journal of headache and pain. 2019;20(1):45.
89. Ayata C, Shimizu-Sasamata M, Lo EH, Noebels JL, Moskowitz MA. Impaired neurotransmitter release and elevated threshold for cortical spreading depression in mice with

mutations in the alpha1A subunit of P/Q type calcium channels. Neuroscience. 2000;95(3):639-45.
90. Jarvis CR, Anderson TR, Andrew RD. Anoxic depolarization mediates acute damage independent of glutamate in neocortical brain slices. Cerebral cortex. 2001;11(3):249-59.
91. Brisson CD, Andrew RD. A neuronal population in hypothalamus that dramatically resists acute ischemic injury compared to neocortex. Journal of neurophysiology. 2012;108(2):419-30.
92. Osehobo EP, Andrew RD. Osmotic effects upon the theta rhythm, a natural brain oscillation in the hippocampal slice. Experimental neurology. 1993;124(2):192-9.
93. Juzekaeva E, Gainutdinov A, Mukhtarov M, Khazipov R. Reappraisal of anoxic spreading depolarization as a terminal event during oxygen-glucose deprivation in brain slices in vitro. Scientific reports. 2020;10(1):18970.
94. Brisson CD, Hsieh YT, Kim D, Jin AY, Andrew RD. Brainstem neurons survive the identical ischemic stress that kills higher neurons: insight to the persistent vegetative state. PloS one. 2014;9(5):e96585.
95. Dreier JP, Reiffurth C. The stroke-migraine depolarization continuum. Neuron. 2015;86(4):902-22.
96. Reiffurth C, Alam M, Zahedi-Khorasani M, Major S, Dreier JP. Na(+)/K(+)-ATPase alpha isoform deficiency results in distinct spreading depolarization phenotypes. Journal of cerebral blood flow and metabolism : official journal of the International Society of Cerebral Blood Flow and Metabolism. 2020;40(3):622-38.
97. Esmann M, Fedosova NU, Marsh D. Osmotic stress and viscous retardation of the Na,K-ATPase ion pump. Biophysical journal. 2008;94(7):2767-76.
98. Hertelendy P, Varga DP, Menyhart A, Bari F, Farkas E. Susceptibility of the cerebral cortex to spreading depolarization in neurological disease states: The impact of aging. Neurochemistry international. 2019;127:125-36.
99. Marshall WH. Spreading cortical depression of Leao. Physiological reviews. 1959;39(2):239-79.
100. Kreisman NR, Soliman S, Gozal D. Regional differences in hypoxic depolarization and swelling in hippocampal slices. Journal of neurophysiology. 2000;83(2):1031-8.
101. Dreier JP, Major S, Foreman B, Winkler MKL, Kang EJ, Milakara D, et al. Terminal spreading depolarization and electrical silence in death of human cerebral cortex. Annals of neurology. 2018;83(2):295-310.
102. Andrew RD, Labron MW, Boehnke SE, Carnduff L, Kirov SA. Physiological evidence that pyramidal neurons lack functional water channels. Cerebral cortex. 2007;17(4):787-802.
103. Nagelhus EA, Mathiisen TM, Ottersen OP. Aquaporin-4 in the central nervous system: cellular and subcellular distribution and coexpression with KIR4.1. Neuroscience. 2004;129(4):905-13.
104. Wilson CS, Mongin AA. Cell Volume Control in Healthy Brain and Neuropathologies. Current topics in membranes. 2018;81:385-455.
105. Stokum JA, Gerzanich V, Simard JM. Molecular pathophysiology of cerebral edema. Journal of cerebral blood flow and metabolism : official journal of the International Society of Cerebral Blood Flow and Metabolism. 2016;36(3):513-38.
106. Wilson CS, Bach MD, Ashkavand Z, Norman KR, Martino N, Adam AP, et al. Metabolic constraints of swelling-activated glutamate release in astrocytes and their implication for ischemic tissue damage. Journal of neurochemistry. 2019;151(2):255-72.
107. Szatkowski M, Barbour B, Attwell D. Non-vesicular release of glutamate from glial cells by reversed electrogenic glutamate uptake. Nature. 1990;348(6300):443-6.

108. Mahmoud S, Gharagozloo M, Simard C, Gris D. Astrocytes Maintain Glutamate Homeostasis in the CNS by Controlling the Balance between Glutamate Uptake and Release. Cells. 2019;8(2).
109. Mei YY, Lee MH, Cheng TC, Hsiao IH, Wu DC, Zhou N. NMDA receptors sustain but do not initiate neuronal depolarization in spreading depolarization. Neurobiology of disease. 2020;145:105071.
110. Enger R, Tang W, Vindedal GF, Jensen V, Johannes Helm P, Sprengel R, et al. Dynamics of Ionic Shifts in Cortical Spreading Depression. Cerebral cortex. 2015;25(11):4469-76.
111. Luckl J, Lemale CL, Kola V, Horst V, Khojasteh U, Oliveira-Ferreira AI, et al. The negative ultraslow potential, electrophysiological correlate of infarction in the human cortex. Brain : a journal of neurology. 2018;141(6):1734-52.
112. Peters O, Schipke CG, Hashimoto Y, Kettenmann H. Different mechanisms promote astrocyte Ca2+ waves and spreading depression in the mouse neocortex. The Journal of neuroscience : the official journal of the Society for Neuroscience. 2003;23(30):9888-96.
113. Chuquet J, Hollender L, Nimchinsky EA. High-resolution in vivo imaging of the neurovascular unit during spreading depression. The Journal of neuroscience : the official journal of the Society for Neuroscience. 2007;27(15):4036-44.
114. Largo C, Cuevas P, Somjen GG, Martin del Rio R, Herreras O. The effect of depressing glial function in rat brain in situ on ion homeostasis, synaptic transmission, and neuron survival. The Journal of neuroscience : the official journal of the Society for Neuroscience. 1996;16(3):1219-29.
115. Bardutzky J, Schwab S. Antiedema therapy in ischemic stroke. Stroke. 2007;38(11):3084-94.
116. Carney N, Totten AM, O'Reilly C, Ullman JS, Hawryluk GW, Bell MJ, et al. Guidelines for the Management of Severe Traumatic Brain Injury, Fourth Edition. Neurosurgery. 2017;80(1):6-15.
117. Jha RM, Kochanek PM, Simard JM. Pathophysiology and treatment of cerebral edema in traumatic brain injury. Neuropharmacology. 2019;145(Pt B):230-46.
118. Schupper AJ, Eagles ME, Neifert SN, Mocco J, Macdonald RL. Lessons from the CONSCIOUS-1 Study. Journal of clinical medicine. 2020;9(9).